Schweizerische Eidgenossenschaft
Confédération suisse
Confederazione Svizzera
Confederaziun svizra

Federal Department of the Environment, Transport, Energy and Communications DETEC

Swiss Federal Office of Energy SFOE
Energy Research and Cleantech Division

Final report dated 31.8.2021

EMeLi

Effizienter Methan-Antrieb für Lieferwagen (Efficient Methane Powertrain for Light Commercial Vehicles)

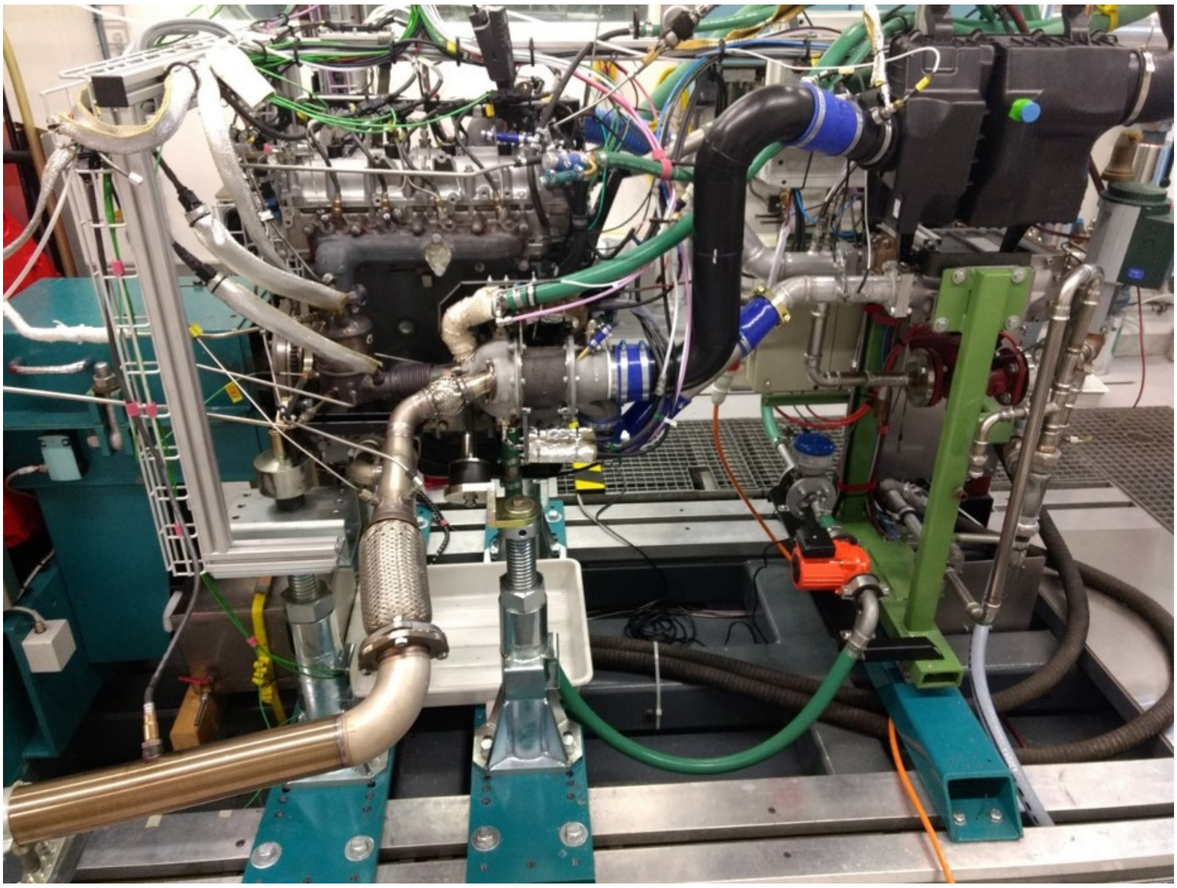

Source: Empa (FPT F1C engine with Comprex™ supercharger at Empa's engine test bench)

Date: 31.08.2021

Location: Bern

Publisher:
Swiss Federal Office of Energy SFOE
Energy Research and Cleantech
CH-3003 Bern
www.bfe.admin.ch

Co-financing:
SCCER Mobility

Subsidy recipients:
Empa, Automotive Powertrain Technologies Laboratory
Überlandstrasse 129, CH-8600 Dübendorf
www.empa.ch/abt504

Authors:
Patrik Soltic, Empa, patrik.soltic@empa.ch
Norbert Zsiga, Empa, norbert.zsiga@empa.ch

SFOE project coordinators:
Luca Castiglioni, luca.castiglioni@bfe.admin.ch

SFOE contract number: SI/501743-01

Summary

The EMeLi project aims to develop tools, methods and technologies to make natural gas internal combustion engines for commercial vehicles more efficient and attractive for the customer. Several key components shall therefore be optimized for the operation with methane. The base engine is the series production FPT F1C CNG Euro VI engine and FPT supports the project with hardware (series production parts as well as prototype parts). The FPT F1C reaches Euro 6 exhaust emission standards and is for example used in the light commercial vehicle Iveco Daily.

In the project, several measures of engine improvement as well as hybridization of the vehicle and their impact on the fuel consumption, driving dynamic and emissions was investigated. The increase of the compression ratio and the use of a Miller camshaft in combination with a pressure wave supercharger are the strongest measures for reduction of the fuel consumption and simultaneous increase of peak torque and peak power output. The use of water injection can help to increase the peak power output significantly without violating given temperature limitations. By means of hybridization, the fuel consumption can be further decreased significantly. By using a smaller (and lighter) internal combustion engine, the additional weight of the electric components can be compensated while the resulting vehicle can still accelerate much more quickly.

The envisaged increase of the maximal torque and power output of 20% each could be achieved within this project. A simultaneous reduction of the fuel consumption of 7% by engine measures alone could be shown. With hybridization, the possible reduction of CO_2 emissions increases to 30% and a mass neutral plugin-hybrid can be built with an all-electric driving range of about 30 km. By means of an ideal combination of engine measures, the (partial) electrification of the drivetrain and a de-fossilisation of the fuel (biogas) the best results can be achieved.

Zusammenfassung

Das Projekt EMeLi hat das Ziel, Werkzeuge, Technologien und Methoden zu entwickeln um Methan-Verbrennungsmotoren für den Einsatz in Lieferwagen attraktiver und effizienter zu machen, Als Basis dient ein Serienmotor (FPT F1C CNG Euro VI), der Hersteller FPT unterstützt das Projekt mit Hardware (Serien- und Prototypenbauteile). Im Projekt wurden sowohl diverse innermotorische Massnahmen als auch die Hybridisierung des Fahrzeugs und ihr Einfluss auf Verbrauch, Fahrdynamik und Emissionsverhalten untersucht. Die Erhöhung des Verdichtungsverhältnisses und die Verwendung einer Miller-Nockenwelle in Verbindung mit einem Druckwellenlader sind die stärksten Massnahmen zur Reduktion des Verbrauchs bei gleichzeitiger Steigerung des maximalen Drehmoments. Die Verwendung einer Wassereinspritzung kann die maximale Leistung deutlich erhöhen ohne Temperaturbegrenzungen zu verletzen. Durch eine Hybridisierung kann der Verbrauch abermals verringert werden. Durch die Verwendung eines kleineren (und leichteren) Verbrennungsmotors kann das Gewicht der elektrischen Komponenten kompensiert werden während das resultierende Fahrzeug immer noch deutlich dynamischer beschleunigen kann.

Die angepeilte Erhöhung des maximalen Drehmomentes sowie der maximalen Leistung um 20% durch motorische Massnahmen konnte erreicht werden. Mit Hybridisierung steigt die mögliche CO_2 Reduktion auf bis zu 30% und ein massen-neutrale PlugIn Hybridvariante mit einer rein elektrischen Reichweite von ca. 30 km ist ebenfalls möglich. Durch eine optimale Kombination von innermotorischen Massnahmen, der (teilweisen) Elektrifizierung des Antriebsstrangs und einer Defossilisierung des Kraftstoffs (Biogas) können die besten Ergebnisse erzielt werden.

Main findings

This project revealed a number of methods/technologies which are suitable for the performance increase and greenhouse gas reduction of natural gas engines used in light commercial vehicles. Using an adequate piston shape (hemi bowl), a diesel-like compression ratio of 16.5 is possible without only minor knock limitations at full load operation. Early intake valve closing, so called Miller valve timing, brings considerable efficiency benefits but also challenges for engine boosting which would traditionally ask for two-stage turbocharging. Two-stage turbocharging is expensive and has a bad transient behaviour, especially in Lambda=1 engine concepts. An alternative boosting method– the Swiss innovation Comprex™ – proves to work excellently and is able to deliver boost levels needed for Miller concepts, also at very low engine speed. Despite the reduction of the effective engine displacement by early intake valve closing, such a Comprex/Miller setup is able to outperform a classical turbo concept by 20% in terms of peak power and peak torque.

Electric hybridization can be used as an add-on, or an alternative to enhanced engine performance. This approach brings the largest benefit in terms of CO_2 reduction, but it decreases also the vehicle's payload – which is critical in commercial vehicles. However, a hybridization concept with a smaller internal combustion engine is possible to be mass-neutral and to provide the largest efficiency increase.

Contents

Abbreviations

SCCER	Swiss Competence Center for Energy Research
CNG	Compressed Natural Gas
FPT	Fiat Powertrain Technologies
TWC	Three Way Catalyst
OC	Oxidation Catalyst
CR	Compression Ratio
CFD	Computational Fluid Dynamics
COC	Center of Combustion
kW	Kilowatt
Nm	Newtonmeter
rpm	rotations per minute
PWS	Pressure wave supercharger
EGR	Exhaust Gas Recirculation
FPT	Fiat Powertrain Technologies
VTG	Variable Turbine Geometry
IMEP	Indicated Mean Effective Pressure
BMEP	Brake Mean Effective Pressure

1 Introduction

1.1 Background information and current situation

The European market of natural gas/biogas powered vehicles is constantly growing. Currently about 1.9 million CNG vehicles are registered in Europe [1]. These are passenger cars, trucks (light duty, medium duty and heavy duty) and buses. In the EU and EFTA countries, more than 4'000 CNG filling stations are in operation and also the number of LNG filling stations is constantly growing with actually around 400 in operation [2]. 17% of the methane sold at filling stations is biomethane in Europe and the gas industry committed to increase this to a European average of 40% by 2030.
However, in Europe, both kinds of regions can be found: such with rich infrastructure and such with complete lack of it. Switzerland has a rather good infrastructure with actually more than 150 filling stations [3]. This dedication of the Swiss gas industry to invest in the natural gas/biogas filling infrastructure gives Switzerland the opportunity to use the advantages [4] of this fuel:

- very low pollutant emissions (including NO_x and PM), also in real-world conditions, due to the possibility of soot-free combustion and three-way catalytic exhaust gas treatment,
- low level of noise compared to diesel engines (especially relevant at low-speed vehicle operation),
- full compatibility with renewable biogenic of synthetic methane.

Currently produced vehicle gas engines are derivatives from petrol or diesel engines, depending on the segment. In both cases, the final result is a compromise between the possibilities offered by the gaseous fuel and the limitations of the particular type of the basic engine. This project concentrates on delivery vans (N1 class according to regulation EC No 595/2009 [5]). These vehicles have typically high annual mileages, are very often used in urban areas and come back to a base each day and refuelling is usually not a problem. Up to now, this class of vehicles is powered mostly with diesel engines. All manufacturers of such vehicles are developing pure battery electric versions which are able to cover daily ranges of typically around 200 km which is enough for many urban applications. However, a large share of such vehicles perform far longer daily trips (internal data from interviews with a number of Swiss companies) which asks for the foreseeable future for solutions with (preferably renewable) chemical energy carriers. Therefore it is very likely, that CNG/biomethane vehicles in this segment will become increasingly important to achieve climate protection goals.

1.2 Purpose of the project

The electrification of the transport sector proceeds continuously, especially with regards to applications with a low continuous power demand such as passenger cars. In other segments of the transport sector, the electrification is significantly more difficult. For trucks, commercial vehicles and mobile machinery, which often need a very large driving range or the high continuous power, the payload or operation time would be significantly reduced by batteries. One possibility for this class of vehicles to reduce the CO_2 emissions is the operation with renewable or low-carbon chemical energy carriers. Methane (CNG / biogas) is such an option which proved to be economically feasible. However, the operation of a methane engine should in any case be as efficient as possible and its performance should be comparable with the well-accepted diesel solutions. This requires a systematic optimization of such engines, which is what this project aims for.

A number of manufacturers offer CNG versions of light and heavy commercial vehicles which are typically derived from diesel engines but, due to low sales volumes, this conversion is done with a comparably low technical effort. Since $\lambda=1$ natural gas combustion concepts are necessary to fulfil the emission standards but lead to higher exhaust temperatures compared to diesel combustion, maximum power is normally limited in order to protect the components derived for the basic diesel engine. This lack of power and torque often leads to rather low acceptance by the drivers. This is also the case for the engine for delivery vans, which is in focus of the present project. This non-optimal setup o results also to a comparably low efficiency, so that, even if the fuel has a lower carbon-content compared to diesel, the resulting CO_2 emissions are higher. The project described here has therefore the task to improve the current technology of CNG/biogas light commercial vehicles in terms of performance and efficiency.

1.3 Objectives

Feedback from drivers of light commercial CNG vehicles is often negative because of a drivability which is worse compared to similar vehicles equipped with highly sophisticated Diesel engines. This project has the CNG powertrain of the Euro 6 Iveco Daily delivery van (Figure 1) in focus which uses the FPT F1C engine.

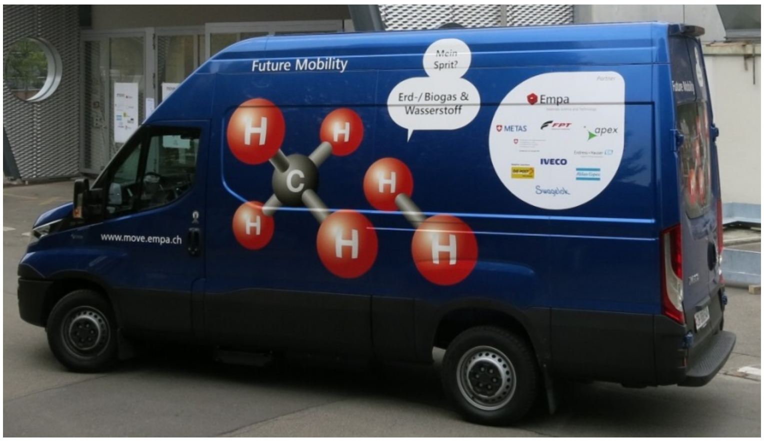

Figure 1: Iveco Daily CNG (Empa's project vehicle for HCNG operation) [Empa]

The objective of the project described here was to develop tools and methods for optimal selection of parameters and optimal design of components for the engine and drivetrain of a delivery van, and validate the measures experimentally. The target of the project was to demonstrate a fuel consumption and CO_2 reduction with these tools and methods by 20% compared to the actual Euro-VI engine and to increase at the same time the maximum power by 20%. Additionally, the project assesses the potential of hybridization in this vehicle segment, using numerical tools.

Figure 2 pictures the current serial production F1C CNG engine, which is a derivate of the F1C diesel version, with its full load characteristics. It shows that the engine delivers a continuous power of 100 kW and has a peak torque level of 350 Nm. In its highest-performing diesel version, this engine delivers 152 kW / 470 Nm (using two-stage turbocharging). The quantitative goal is therefore to increase the CNG engine's continuous peak power to at least 120 kW, which also means to increase the engine's peak torque adequately. Such measures lead to a driveability which is comparable with a diesel engine.

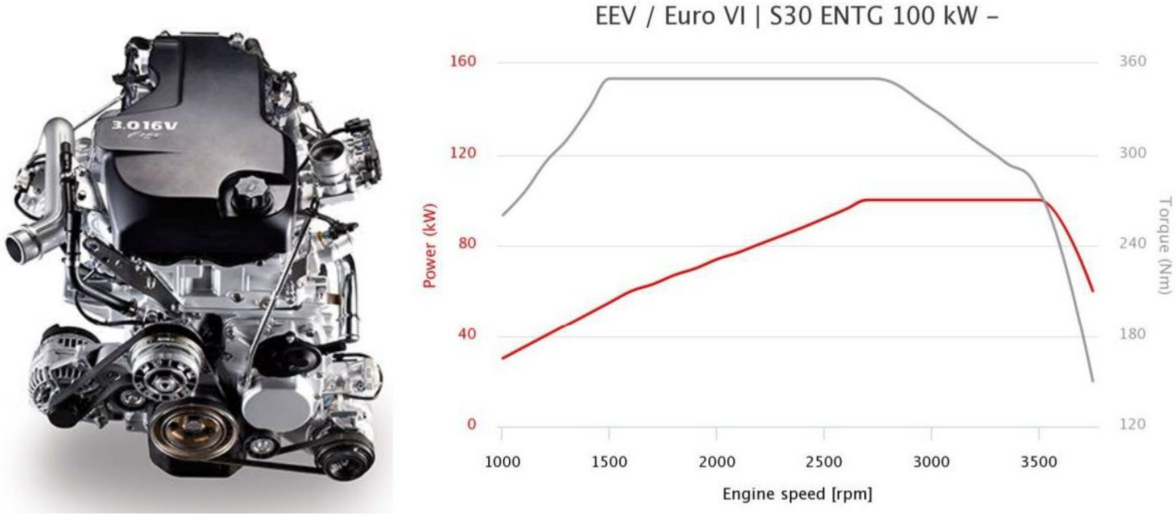

Figure 2: Full load characteristics of the serial production FPT F1C CNG engine [6].

2 Description of facility

Experiments were performed on an engine test bench at Empa with the aforementioned FPT F1C engine with four cylinders and a displacement of 3.0 litres in a number of different configurations, as described later. The engine was operated with port-fuel-injected natural gas (CNG) and was controlled to stoichiometric conditions. To have the full flexibility for configuration changes, the engine was equipped with an in-house developed control architecture, based on a commercially available rapid prototyping platform.

Table 1 gives an overview of the experimental setup. In order to assess the possibilities to increase its efficiency, pistons with different compression ratios and bowl shapes were used. A high pressure exhaust gas recirculation (EGR) path was implemented. Three different camshafts in addition to the conventional camshaft were available, as well. Two of them have Miller valve timing with an early intake valve closing angle and the third has Atkinson valve timing with a late intake valve closing angle. Furthermore, the engine was equipped with water injection to test its cooling effect on the peak power output and its knock mitigation capabilities. Also, a set pf prechamber spark plugs could be used as an alternative to the conventional spark plugs. Finally, a pressure wave supercharger was produced and was also available as an alternative boosting device to the turbocharger used in the serial-production-state of the engine.

Table 1: Main characteristics of the used engine configuration(s) and the test bench

Engine Basis	FPT F1C 3.0 liter, CNG version
Bore/Stroke/number of cylinders	96.0mm / 104.0mm / 4
Compression Ratios	11.5, 12.5 (standard), 13.5, 14.5, 16.5
Fuelling	Port fuel injection of natural gas, Bosch NGI2 Injectors
Variability in the valve train	none (fixed lift, no valve timing adjustment)

Conventional camshaft intake	max. lift 8.5mm, intake valve closing angle 565◦CA
Miller camshaft intake	max. lift 6.1mm, intake valve closing angle 525◦CA
Miller camshaft 2 intake	max. lift 4.8mm, intake valve closing angle 500◦CA
Atkinson camshaft intake	max. lift 8.5mm, intake valve closing angle 606◦CA
Cylinder head	Two versions: high swirl and low swirl
Charge air intercooler	water/air intercooler, fixed water mass flow rate and constant water inlet temperature
Turbocharger	Garrett compressor and turbine
Pressure wave supercharger	Antrova Comprex™ D114/L112
Comprex drive motor	Electric, 1.24kW peak power
Exhaust Gas Recirculation (EGR)	Configuration without EGR, configuration with high-pressure EGR with EGR cooler (and EGR cooler bypass possibility)
Port water injectrors	Nostrum Energy
Engine control	In-house developed, rapid-prototyping system (dSPACE)
In-cylinder pressure transducers	M5 piezoelectric, (Kistler 6054BRS32U) in all cylinders
Lambda sensors	Wide band (Bosch LSU 4.9)
Emission measurements	Horiba Mexa 7400 certification-grade emission bench with two sampling lines, V&F Analyse- und Messtechnik GmbH HSense mass spectrometer, AVL SESAM FTIR spectrometer
Fuel flow measurement	Coriolis (Rheonik RHM015/RHE07)
Combustion air flow measurement	ABB Sensyflow FMT700-P
Torque measurement	GIF torque transducer
Flywheel / gearbox	Standard / no gearbox

The engine was operated using natural gas from the Swiss gas grid and the gas was analysed using a gas chromatograph (Siemens MicroSAM). Crank-angle-based and time-based data was recorded with a Kistler KiBox indication platform as well the test bench's automation system SRH STARS, respectively. The temperatures and pressures were measured at various locations along the intake and exhaust gas flow paths, and especially upstream and downstream of each catalytic converter and components of the charging devices. The emissions measurement equipment was used to analyse the exhaust gas upstream and downstream of each catalytic converter.

The boosting device, the intake camshafts and the pistons were be changed and allow the analysis of the performance of the engine. Figure 3 shows pictures of the engine in its turbocharger as well as in its Comprex setup.

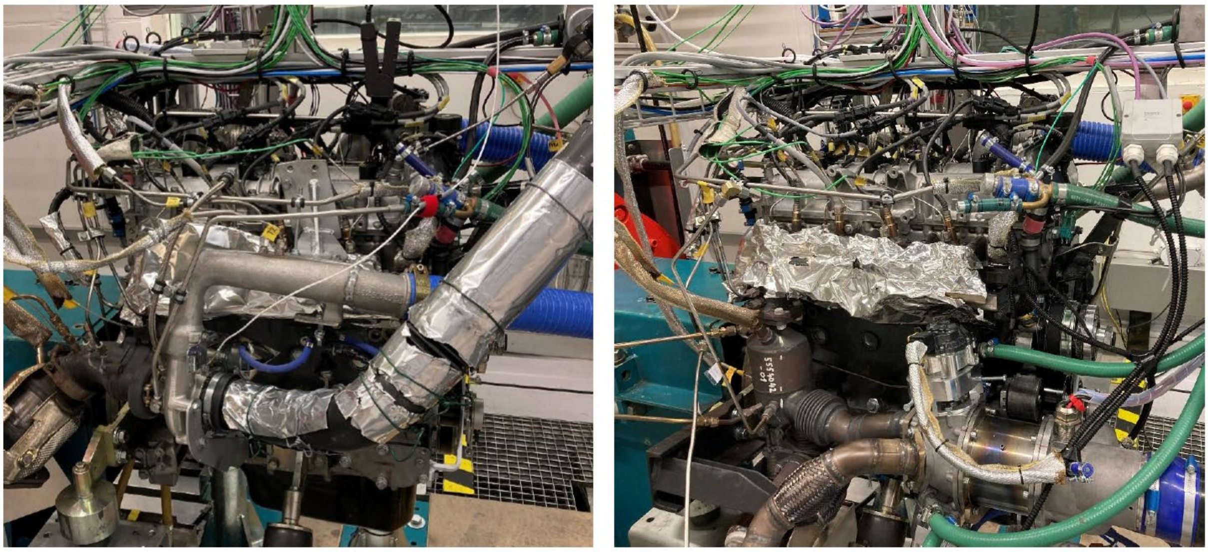

Figure 3: Photographs of the engine equipped with a turbocharger (left) and a Comprex (right)

3 Procedures and methodology

In this project experimental as well as simulative analyses were carried out. A large part of the project was about the optimization of the internal combustion engine itself, a smaller part is about the hybridization of the drive train. Finally, the fuel consumption reduction potential of each measure was analyzed.

The optimization of the internal combustion engine is for the largest part experimental work which was accompanied by computational fluid dynamics simulations performed in cooperation with Politecnico di Milano [7] [8] (including a common PhD thesis of PoliMi and Empa of Giovanni Gianetti). Based on data measured at the test bench simulation model are derived. These models help to understand certain processes in the internal combustion engine and to improve them. The verification and quantification of these measures is again experimental.

The operating data gathered from measurements is also the baseline for the generation on models of the entire vehicle. In this fashion, the fuel consumption in driving cycles and an adaptation of the gearshift strategy can be analysed. Also, a possible hybridisation and the corresponding reduction in fuel consumption and performance gains can be analysed in this fashion, as well.

Regarding adaptations of the internal combustion engine the measurement of several variables to determine the efficiency allow to monitor the success of the measures tested. The effectiveness of measures regarding the drivetrain of vehicle are monitored by means of simulation of fuel consumption in driving cycles.

4 Results and discussion

In the following sections, the approaches and results are presented and discussed.

4.1 1-dimensional engine model

A one dimensional engine model, shown in Figure 4, was adapted, parametrized and validated using measured data of the engine (including for example three-pressure-calibration of the combustion). This model was later used to select the designs for the camshafts to be tested especially in combination with the Comprex pressure wave supercharger.

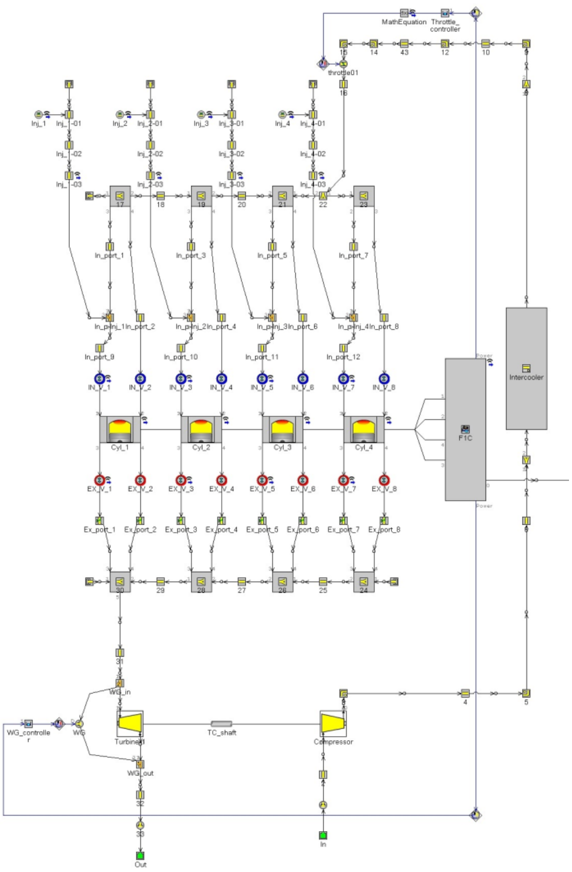

Figure 4: 1D engine model in the simulation software GT-Power [9]

We do not explain the details of this model here as this does not give a benefit in explaining the project’s results.

4.2 Variation of Swirl level, Compression Ratio and Spark Plugs

As an alternative to the classical spark plugs with open hook electrodes in the combustion chambers, passive prechamber spark plugs were assessed. The theoretical advantage of prechambers is that the ignition and early flame kernel development process is decoupled from the often harsh flow motion in the main chamber. This often leads to better flammability, less cyclic variations and a higher tolerance to dilution [10][11][12].

The passive prechamber spark plugs [13] that were used in this project are shown in Figure 5. It is a five-hole design where four jets leaving are leaving the prechamber tangentially and one jet towards the bottom.

Figure 5: Picture of the passive prechamber spark plug used

The volume of the prechamber is around 0.6cm^3 and the electrode is located centrally in the prechamber and has four electrode arms.

Measurements were made using the high swirl cylinder head. Both spark plugs (prechamber and conventional) were tested and the compression ratios (CR) 12.5, 13.5 and 14.5 are compared here at various engine speeds and loads. Figure 6 gives an overview of the operating points.

8°CA centre of combustion gives the highest engine efficiency. At the high loads the engine was operated with a delayed centre of combustion at the border of onset of knock whereas otherwise the optimal centre of combustion of 8°CA after top dead centre could be used.

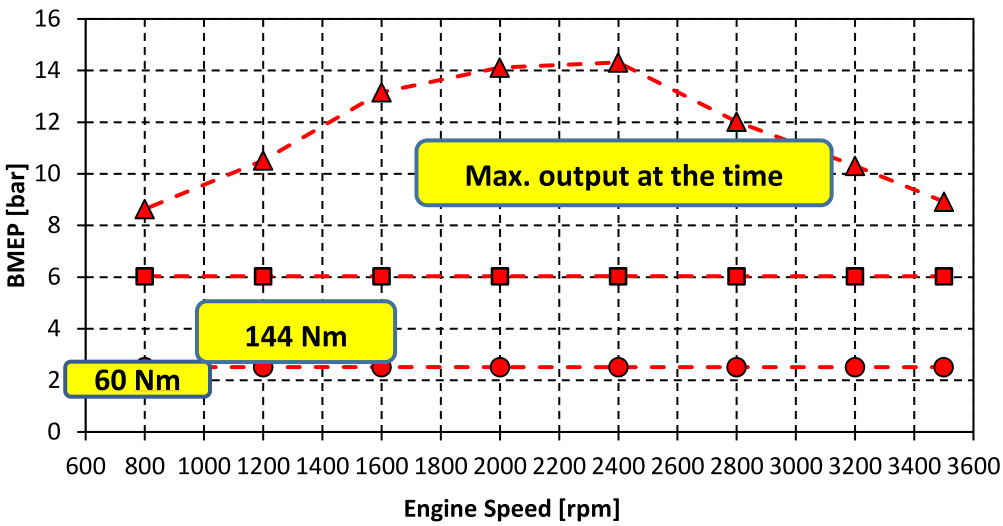

Figure 6: operating points for these analyses

The maximum output at the early stage of the project was limited by the cylinder head temperature, caused by the cooling layout directly derived from the diesel engine. This is the reason why initially, only 14bar brake mean effective pressure (BMEP) were achieved which corresponds to a torque of

332Nm. The maximum power of 84kW is also short of the engine specification of 100kW. This problem was resolved at a later stage of the project when FPT re-designed the cooling channels in the cylinder head which was then prototype-casted for the later experiments (see following section).

The high-load results showed, that compared to the baseline with a compression ratio of 12.5, all other variants tested lead to a higher brake efficiency (see Figure 7). Comparing the conventional spark plugs, increasing the compression ratio to 13.5 gives rather large benefits, whereas a further increase to 14.5 still increases the efficiency, but not as much. Except for high engine speeds, the use of the prechamber spark plugs leads to an additional increase in efficiency for both compression ratios at which they were tested.

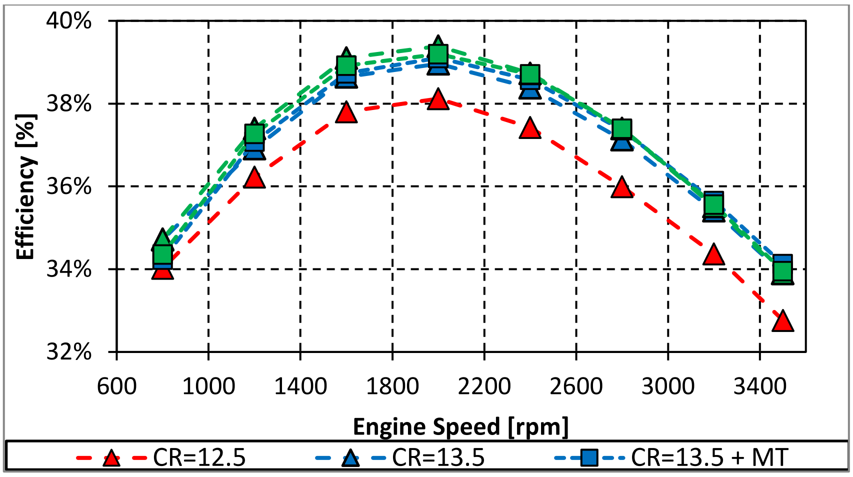

Figure 7: High load results

Figure 8 shows the results for medium and low loads. The compression ratio of 12.5 shows a significantly lower efficiency for both loads and for all configurations tested. There is still a benefit when the prechamber spark plugs are used except for the lowest engine speed tested. However, other than for the high loads, the CR14.5 results are not generally better than the CR 13.5 results at these lower loads. Especially at the low load tests, there is now a small disadvantage for the highest compression ratio.

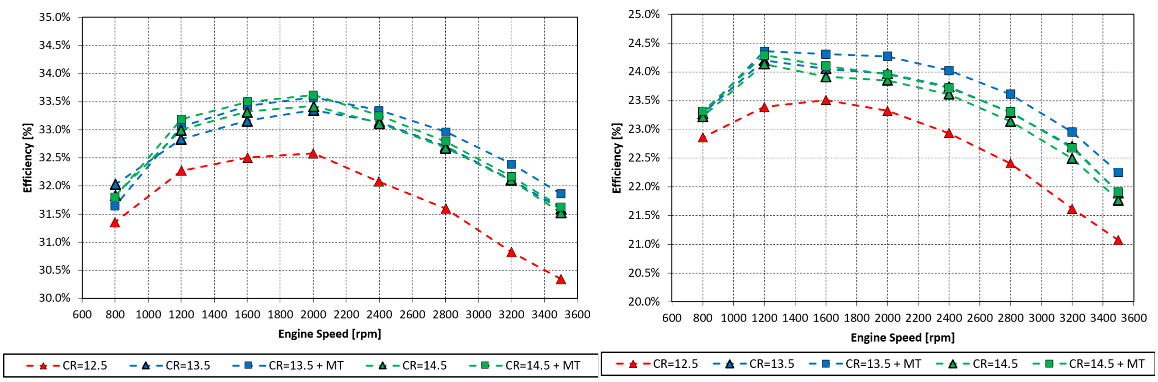

Figure 8: Medium load results (144Nm, left) and low load results (60Nm, right)

The reason for the benefits with use of the Multitorch spark plugs is shown in Figure 9. An increase of the compression ratio and the use of the prechamber spark plugs both lead to a shortened combustion duration. A shorter combustion duration, in combination with a higher compression ratio, in turn is typically beneficial for the efficiency.

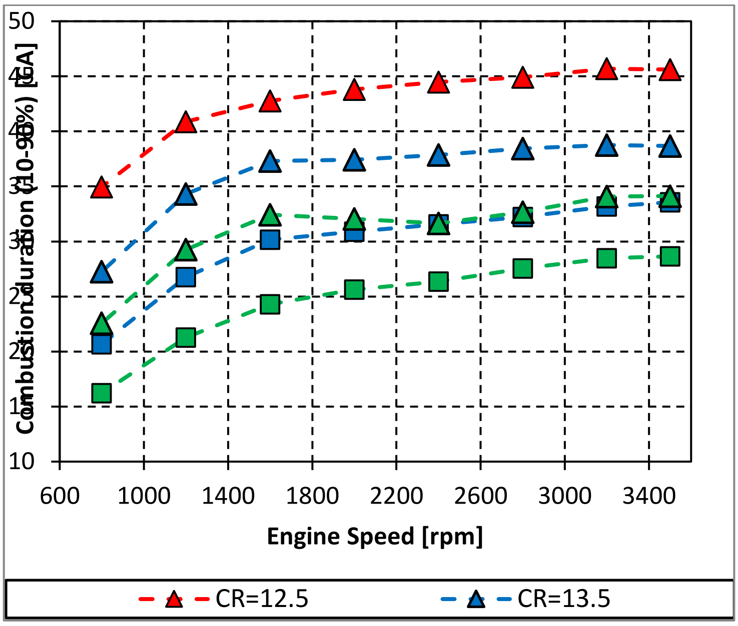

Figure 9: Combustion duration at 144Nm

4.3 Split core cylinder head

The maximum cylinder head temperature (between the exhaust valves), that occurred during the maximum power output measurements detailed in section 4.2, is shown in Figure 10. The temperature increased up to an engine speed of 2400 min^{-1} where it hits the allowed level of around 250°C. For speeds above 2400 min^{-1}, the engine's power output had to be limited to approximately 84kW in order to not exceed this temperature boundary.

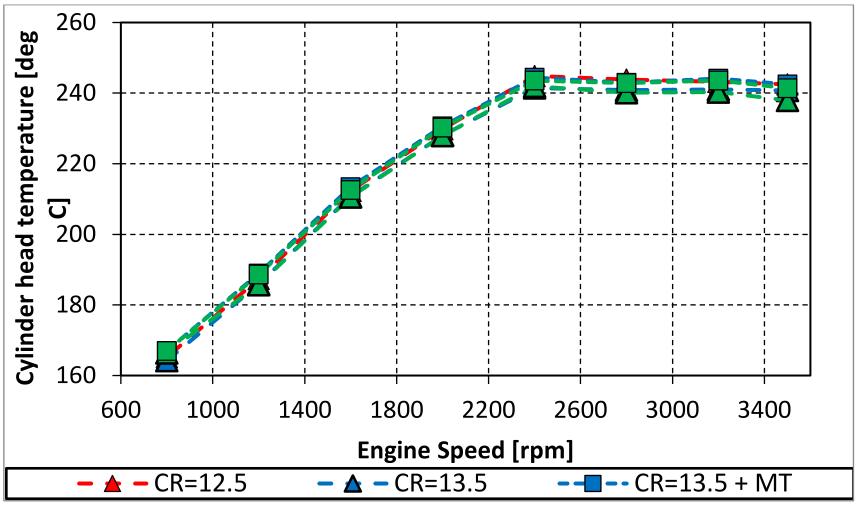

Figure 10: Cylinder head temperature during the measurements described in the previous section

Despite slight differences between the configurations of up to 3°C, the main message of this figure is that the temperature level is too high to increase the power any further.

In order to solve this problem, a split core cylinder head was design and prototype-casted by FPT which had improved cooling channels. This cylinder head was tested both at FPT and at Empa to check if the correct coolant flow was reached and to compare the resulting temperatures (see Figure 11).

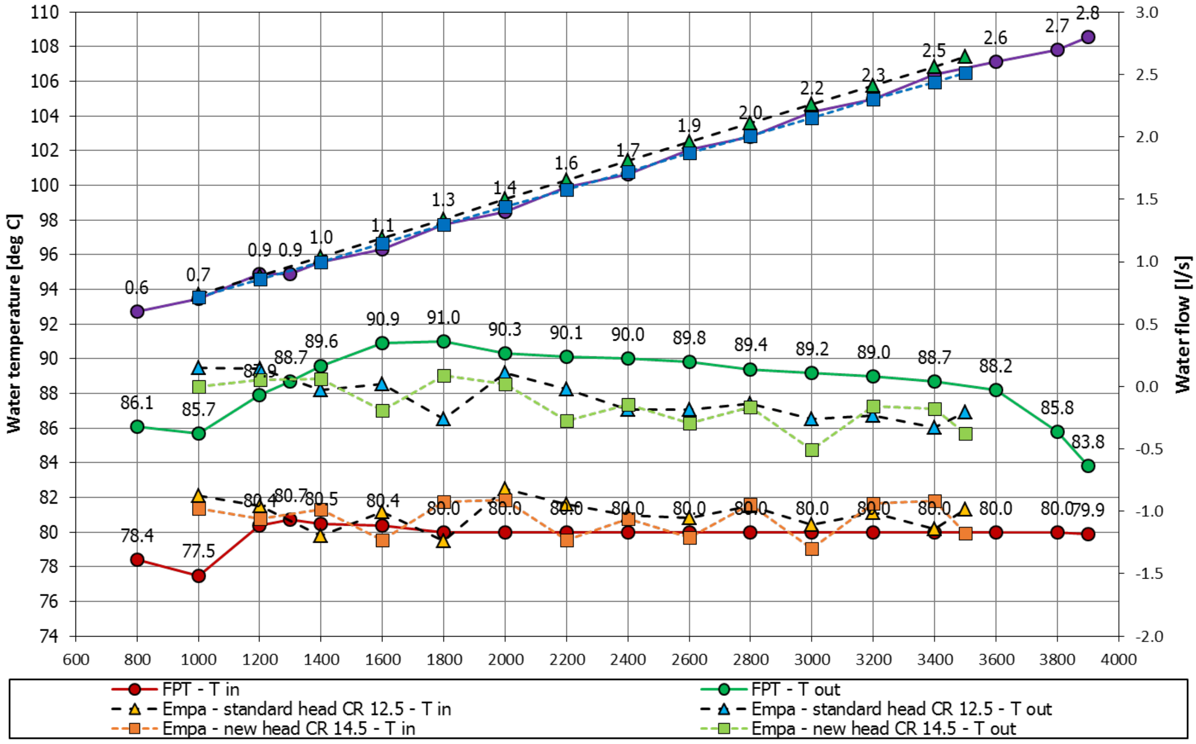

Figure 11: temperatures of the split core cylinder head and coolant flow, measured at FPT and Empa

The full load measurements were repeated. With the enhanced cylinder head, 100 kW continuous peak power and 350 Nm peak torque were reached without any temperature limitations. The results of the cylinder head temperature are shown in Figure 12. In some engine speed range, the cylinder head temperature is up to 25K lower, despite the fact that a higher torque output was obtained. In the peak power engine speed range (engine speeds ≥2750rpm) the cylinder head temperature is approximately 10K lower, even though the torque output is higher by approximately 50Nm.

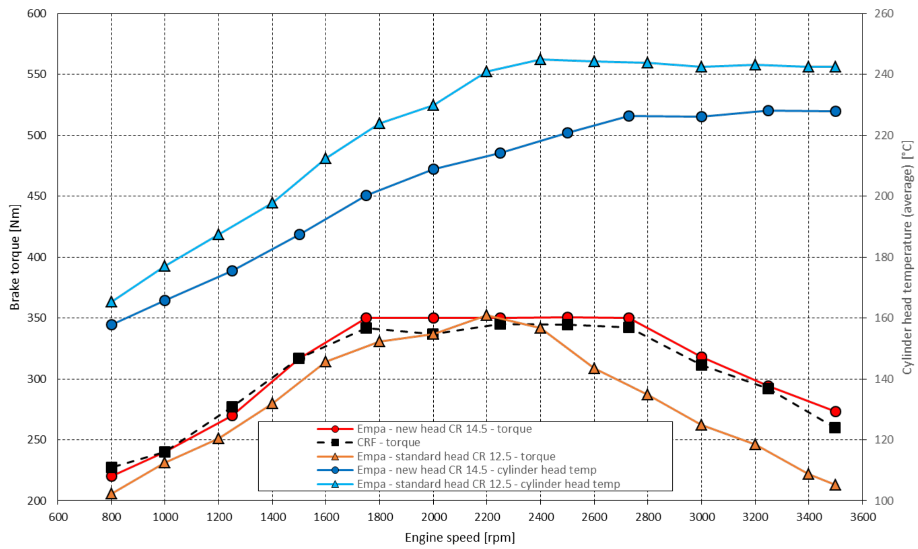

Figure 12: resulting cylinder head temperature with the improved split core cylinder head.

This split core cylinder head was then used in all further measurements and is a key component when it comes to increase the maximum power output of the engine as it was the intention of this project.

4.4 Design of an intake manifold for operation with EGR

In order to operate the engine with EGR, a high pressure EGR system along with a new intake manifold was designed at FPT. The Engine equipped with the EGR system is shown in Figure 13. There is an EGR cooler, as well as a bypass around the EGR cooler in order to provide the possibility to test operation with both hot and cold EGR.

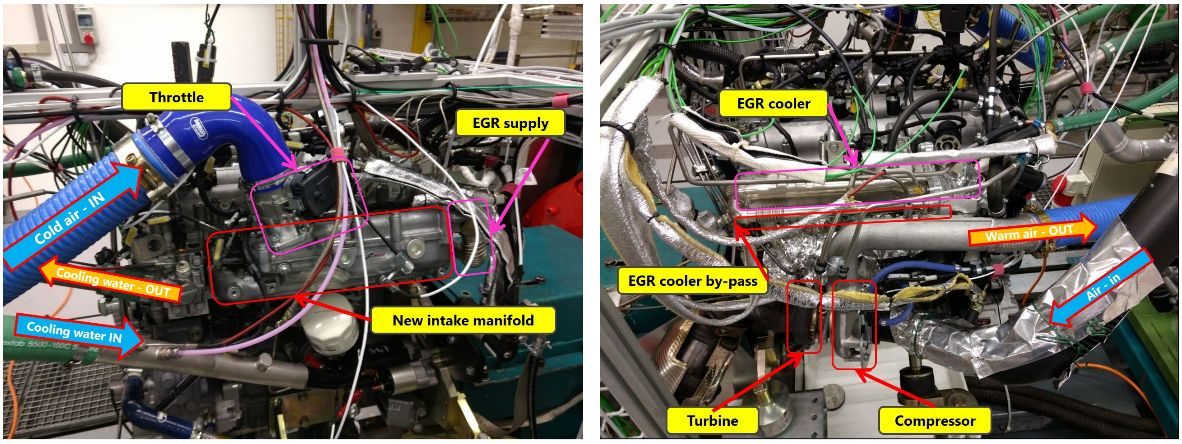

Figure 13: Fotos of the engine equipped with the high pressure EGR system. Intake view (left) and exhaust view (right).

4.5 EGR results

Exhaust gas recirculation (EGR) is mainly used in diesel engines for the reduction of NOx emissions. However, EGR can have advantages also in premixed combustion to lower peak temperatures and, more importantly, to dilute the fresh gas in part load operation in order to reduce throttling losses.

The engine was operated with different EGR-rates at various engine speeds and loads. Due to the differences in combustion properties when EGR is used. These tests were done with the conventional, as well as with prechamber spark plugs. Since EGR is most beneficial in part load condition, we describe here only a part load case (2000 min^{-1}, 102 Nm).

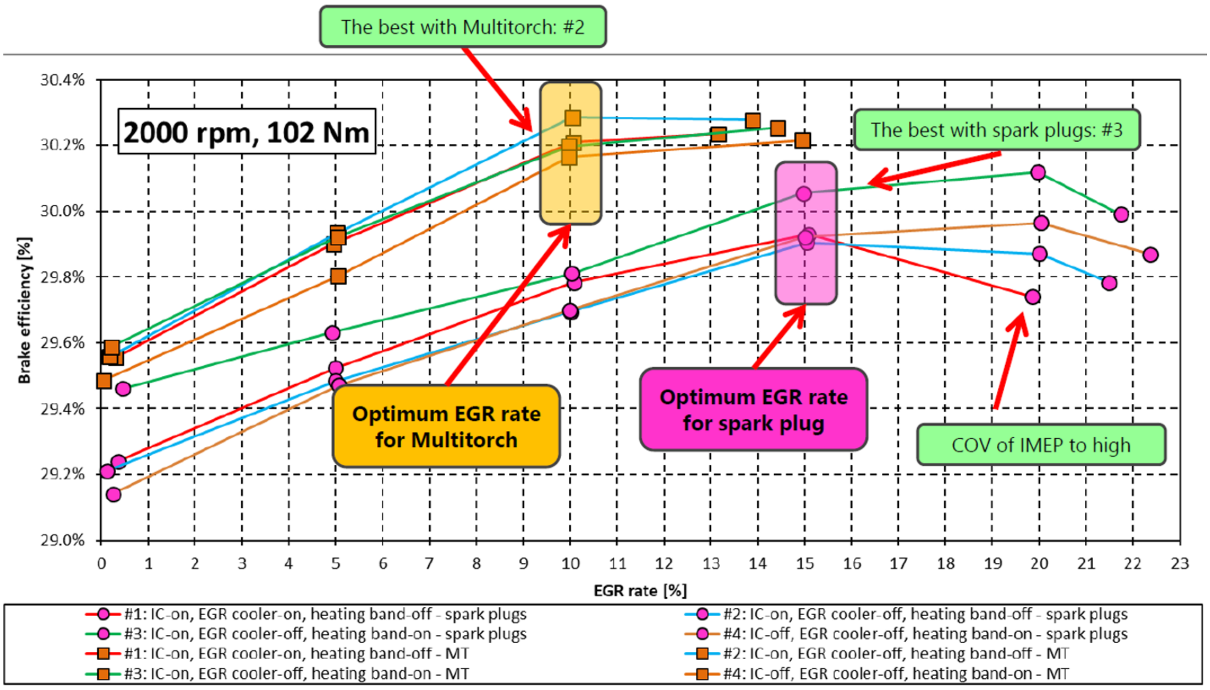

Figure 14: EGR results at a part load operating point for conventional- and prechamber spark plugs

Figure 14 shows that with increasing EGR rates the brake efficiency also increases up to a certain point. The optimal EGR rate when spark plugs are used is 15% whereas the highest efficiency is reached already at an EGR rate of 10% when the prechamber spark plugs are used. As previously shown, the use of prechamber spark plugs leads to a higher efficiency and this is still correct when EGR is used. A further increase of the EGR rate does not lead to further improvements in the efficiency but the combustion stability suffers from a too high EGR rate and the covariance of the indicated mean effective pressure (IMEP) gets worse. Overall, the use of EGR can increase the efficiency by up to 0.8% and in combination with the prechamber spark plugs the efficiency increases by up to 1.0%.

With regards to emissions, it was observed, that the NOx and CO emissions are reduced with EGR whereas the THC emissions increase due to higher flame quenching distances.

4.6 Variation of the piston bowl shape

Figure 15: The different piston shapes: Tower (foreground), Star (middle) and hemispherical (background).

In order to influence the combustion properties, e.g. the raw emissions and the knock tendency, the piston bowl shape can be varied. Giovanni Gianetti designed 2 new piston shapes for his dissertation at Politecnico di Milano by means of 3D CFD simulation. The impact of these new piston shapes was analyzed experimentally at Empa.

Figure 15 shows the different piston geometries, the conventional hemi-shape is shown in the background. These pistons all have a geometrical compression ratio of 14.5.

Measurements were made in the entire engine operating map from 50Nm to 350Nm to compare the different shapes and to quantify, whether the trends that could be seen in CFD simulations could be confirmed experimentally.

The engine was always operated stoichiometrically and the centre of combustion was set at an efficiency optimal 8°CA when possible. At high loads, a later centre of combustion resulted due to knocking and at those operating points the engine was operated at the onset of knock.

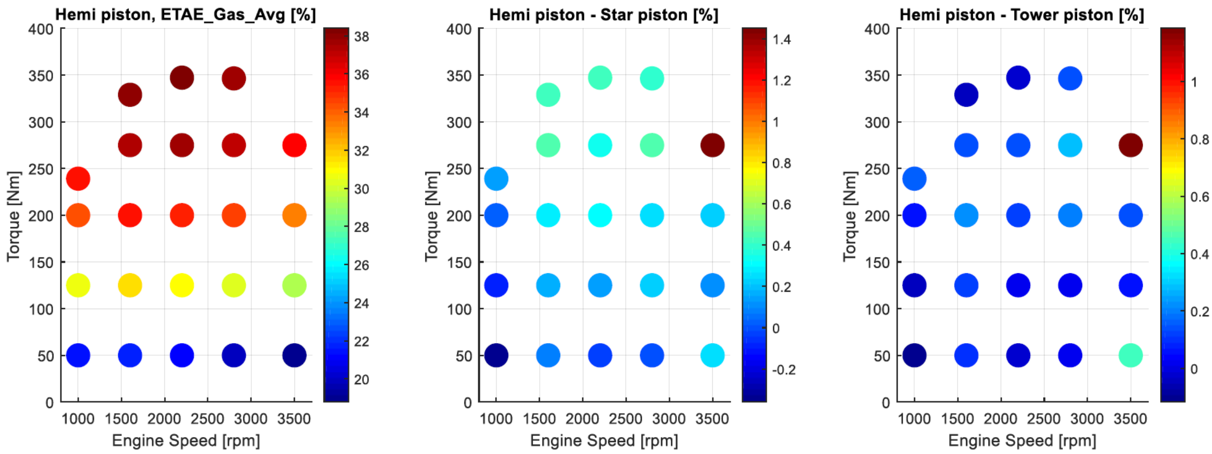

Figure 16: brake efficiency in the entire operating range for different pistons.

Figure 16 shows the resulting brake efficiency values with the different pistons. The data is displayed such that the result of the hemi piston is shown on the left-hand side with the brake efficiency values that were achieved as a basis for the comparison. The middle and right plot each show the difference between the hemi piston and the star piston/tower piston respectively. If the difference is negative, the efficiency is higher for the new design(s). The results show that for both the star piston and the tower piston the efficiency is only better is a very limited part of the engine operating map at low speeds and low loads. In addition to that, the tower piston is also better/equal at low engine speed and high loads. However, in the rest of the operating map, the new piston designs show a slightly lower efficiency.

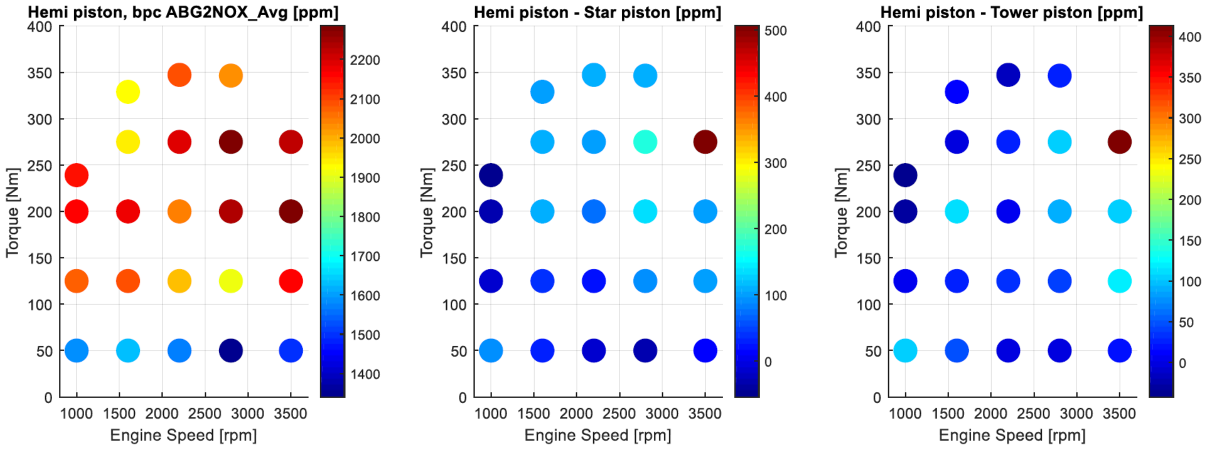

Figure 17: NOx raw emissions in the entire operating range for different pistons.

Figure 17 shows in similar fashion the comparison of the NOx raw emissions. In this case, a difference >0 is advantageous, since low emissions are desirable. Both star and tower piston show small advantages in most of the operating map.

The results of the piston variation are in particular interesting for our project partner Politecnico di Milano for the matching of CFD simulation models to the experimental results. Another important insight is that no significant benefit can be achieved by changing of the piston shape, especially concerning the efficiency and especially, that the standard hemispherical piston shape works best at high loads already. The reason is that turbulence-enhancing piston bowl geometries are able to accelerate combustion (beneficial effect) but they simultaneously increase the wall heat transfer (detrimental effect) so that the net effect is +/- neutral.

Further measurements were carried out in order to find the maximum possible engine torque with each piston at 11 engine speeds between 1000 and 3500min^{-1}, the latest allowed center of combustion was 15°CA for comparison. The limiting factors at these measurement series were a lack of boost pressure, knocking or too high temperatures (exhaust gas or cylinder head).

It must be noted that the 15°CA for the center of combustion are chosen arbitrarily and this helps to compare the pistons among each other. In later measurement series, a center of combustion of up to 20° will be allowed.

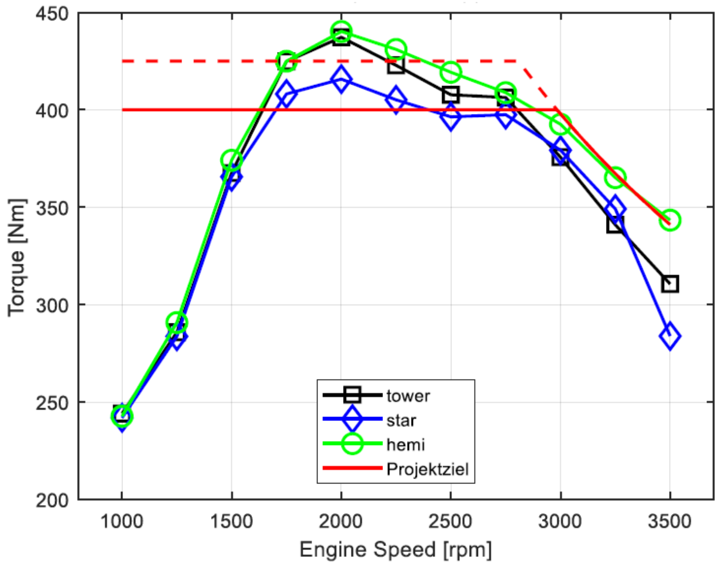

Figure 18: Full load operation with the different piston shapes.

Figure 18 shows the torque values that could be reached with each piston under the given boundary conditions and limitations. At low engine speeds ≤1500min^{-1} the results are similar. The reason is that at these engine speeds not enough boost pressure can be build up despite a fully closed waste gate. At higher engine speeds, knocking is the limiting factor. At engine speeds ≥1750min^{-1} a late center of combustion must be chosen and the engine is operated at the onset of knock. Here, the different piston shapes reach significantly different results. The reason is that the piston shape alters the flow conditions before and during the combustion and in combination with the piston surface temperature, this affects the knock properties. At engine speeds ≥3000min^{-1} the engine reaches a power output of 125kW with the hemi piston. This corresponds to an increase of 25% which is in excess of the project goal of 20%. With the tower and star piston, however, knocking is limiting and a lower power output can be reached.

The best piston shape is the hemispherical shape and all further analyses are done with this piston shape.

4.7 Further increase of the compression ratio

In order to find out if a further increase of the compression ratio still leads to an increase in efficiency, an additional piston was designed with a compression ratio of 16.5 and a hemispherical shape.

Especially for future analyses where Miller/Atkinson camshafts will be used, a further increase of the geometrical compression ratio may be beneficial as the effective one will be reduced by early/late intake valve closing.

As a basis, an operating map was measured for both pistons with the conventional camshaft. Figure 19 shows the resulting efficiency with the CR16.5 piston on the left hand side and the difference to the CR14.5 piston on the right hand side. The results show that at low loads and at low speeds/high loads, there is a slight disadvantage for the high compression ratio piston. However, in the rest of the operating map, the high compression ratio is beneficial.

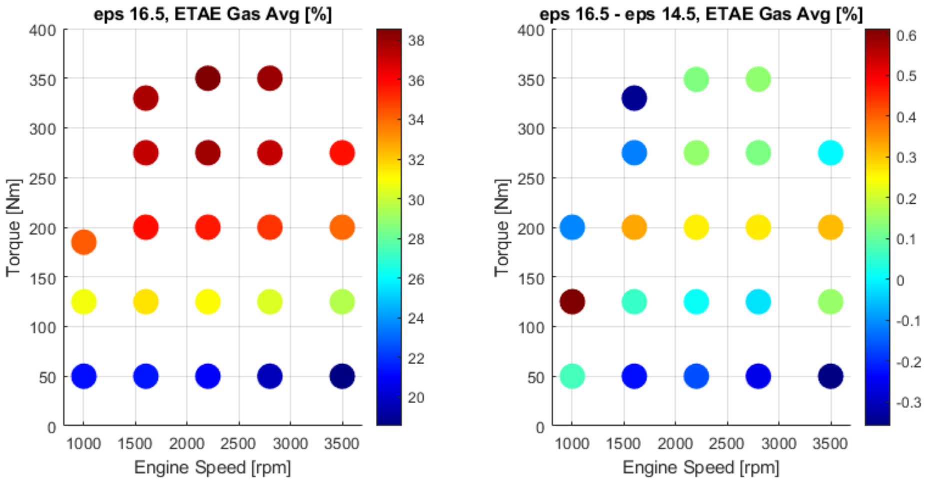

Figure 19: comparison of efficiency with CR16.5 and CR14.5

A further reason to use the CR16.5 piston is to have the "worst case scenario" for full load operation regarding knock. Since later in the project water injection shall be investigated, a high compression ratio should help to show the benefits of that measure.

However: in reality, the engine may also have to be operated with gasoline as an emergency fuel. This may be a limiting factor for the increase of the compression ratio or lead to a decreased power output in gasoline operation when the high compression ratio is used. However, the operation with gasoline is only a very small fraction of the time in a monovalent CNG engine and therefore a temporarily reduced power output should be acceptable.

4.8 Prechamber spark plugs at high loads

As the improved cylinder head is used, higher torque values are now possible at higher engine speeds. In addition, using the Comprex pressure wave supercharger (which will be presented below) a high torque is also possible at low engine speeds. To revisit the prechamber spark plugs at high loads, an additional measurement series has been carried out at 350Nm from 1250 min^{-1} to 2750min^{-1}.

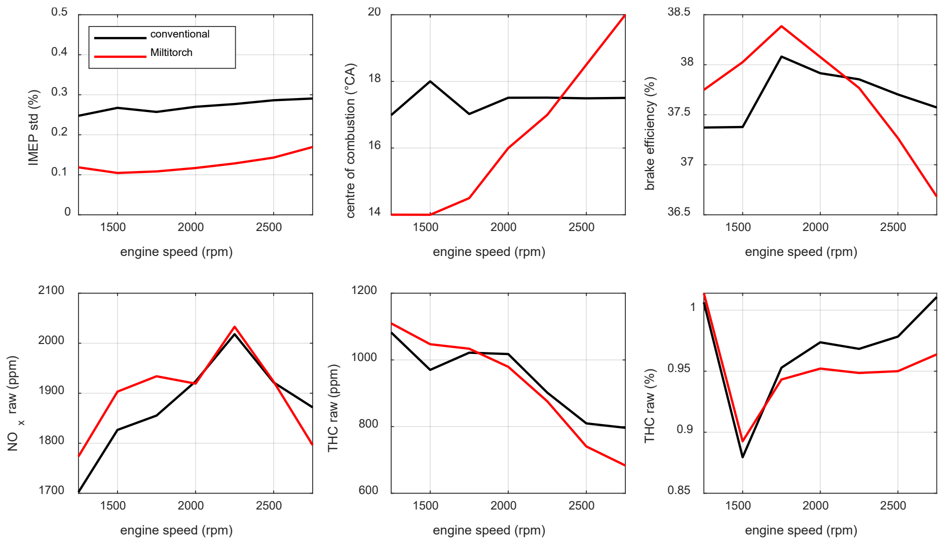

Figure 20: comparison of conventional and prechamber (Multitorch) spark plugs at a torque of 350Nm

Figure 20 shows in the top left plot that for all engine speeds the combustion stability is better when the prechamber spark plugs are used (lower standard deviation of the indicated mean effective pressure IMEP). The upper middle and right plot show the chosen centre of combustion and the resulting brake efficiency. Up to an engine speed of 2250 min^{-1} an earlier centre of combustion can be chosen and the resulting efficiency is higher with the prechamber spark plugs. At higher engine speeds, this trend reverses. The bottom three plots show the raw emissions of NOX, THC and CO, respectively. The emissions are similar for the two ignition systems.

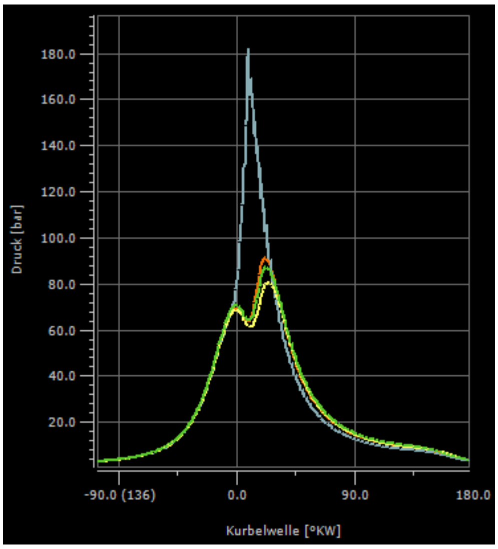

Figure 21: pressure traces during a pre-ignition with the prechamber spark plug

The reason that a later centre of combustion has to be chosen with the Multitorch spark plugs is shown in Figure 21. While three cylinders operate normal in this plot, the pressure trace of one cylinder indicates that a pre-ignition takes place. The pressure of that cylinder starts to increase even before the ignition takes place, which means there is a hot-spot somewhere in the combustion chamber that starts the combustion. Since this does not happen with the conventional spark plugs, it is likely that the hot-spot is located on the prechamber.

The conventional "recipe" to deal with knock (later centre of combustion → less knock) does not work just as well with the prechamber spark plugs. A later centre of combustion does not affect the occurrence of these pre-ignition phenomena in the same way. These phenomena are rare but severe if they occur and may be avoided by shifting the centre of combustion but not always. Initially, these measurements had been planned at 400Nm. However, due to the fact that the knocking was too severe already at 1500min^{-1}, this could not be completed. In order to get the full benefits of the prechamber spark plugs a redesign may be necessary for this particular engine. Since they do lead to an increased efficiency in large parts of the operating map but the technology will not be applicable, as long as these phenomena at high loads are not under control.

4.9 Variation of camshafts

Numerous camshafts had been analysed using the 1D simulation model shown in section 4.1 in order to select the best candidates for engine testing. The three candidates that were tested on the engine are shown in Figure 22.

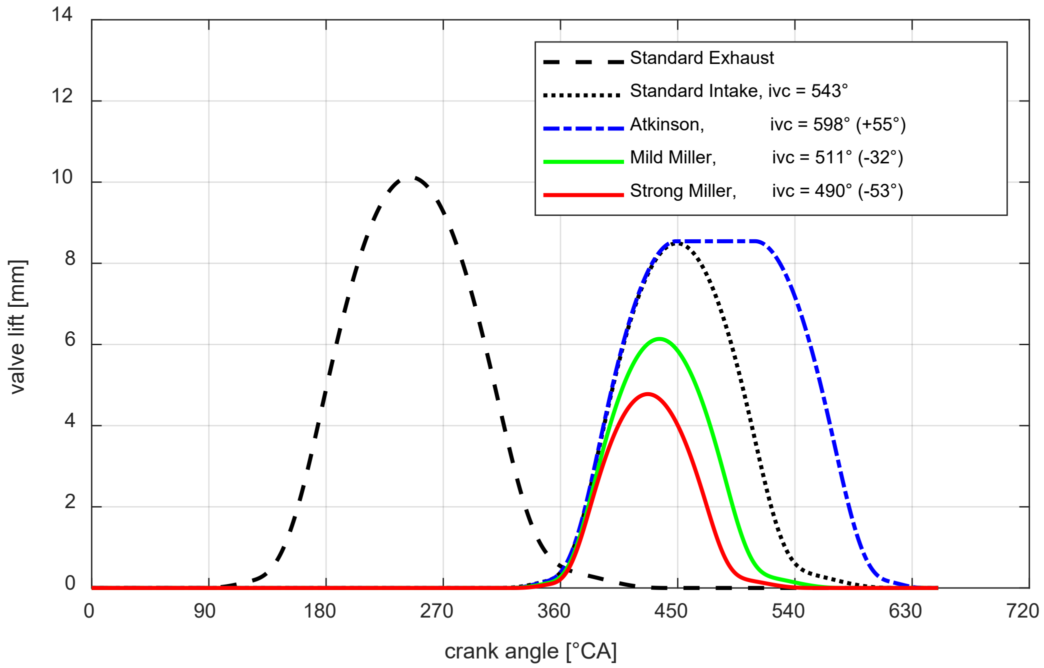

Figure 22: valve lift curves of standard and planned intake camshafts.

When the Atkinson (late intake valve closing) camshaft was used, the results were humbling. Due to the fact that the intake valve closing angle is located significantly after bottom dead centre, mixture is pushed back into the intake manifold during the upward motion of the piston. Due to the geometry of the intake manifold of this particular engine, this mixture is then distributed very unevenly between the cylinders which could be seen in significantly different air to fuel ratios between the cylinders. This problem could to some extent be avoided when the air-to-fuel ratio of each cylinder was controlled individually. However, in addition to that, the stability of the combustion was low and depending on the operating point, frequent misfires occurred. Therefore, this camshaft could not be tested as desired in the entire operating range. The use of such an Atkinson valve timing scheme would need a complete redesign of the intake side (intake channels, intake runner/intake manifold) of the engine with extensive CFD work. This task could not be done within this project.

When the "strong Miller" camshaft was used, these problems did not occur. There were no misfires, but the combustion deteriorated significantly, so that the efficiency benefits were reduced. In addition to that, this camshaft lead to such a strong decrease of the low-end torque that a torque of 350Nm was only possible at 2800min^{-1}.

The "mild Miller" camshaft, however, lead to good results. Due to the dethrottling effect, the pumping losses could be reduced in part load operation and the reduction of the low-end torque, still with the standard turbocharger of this engine, was still noticeable but manageable.

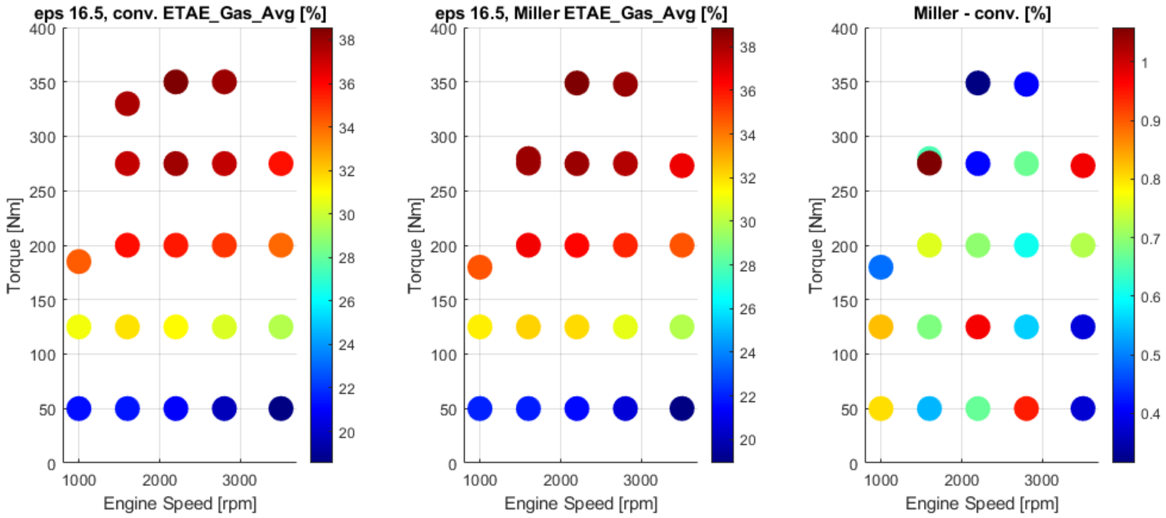

Figure 23: brake efficiency results for conventional camshaft and Miller camshaft

Figure 23 shows that in the entire operating range, the efficiency increases by 0.35%...1.05%. At 1600min^{-1} the brake torque of 330Nm is no longer possible. However, with respect to the torque this effect can be overcompensated with an adapted boosting device as will be shown in the following chapter.

In light of these results, there are only two real options for further comparisons: the conventional camshaft and the "mild Miller" camshaft, which is hereafter referred to as "Miller camshaft" for convenience.

4.10 Pressure wave supercharger as an alternative boosting device

Boosting is a very effective measure to enhance engine efficiency and power density. The main device used for boosting is the turbocharger, invented in 1905 by Alfred Büchi (Sulzer, Switzerland). A turbocharger has the big advantage that it is a comparably simple-to-use device as the exhaust- and the fresh air flow are completely separated by the use of a turbine, coupled to a compressor. The disadvantage of a turbocharger is that, since the compressor is a continuous flow machine, the maximum pressure ratio is limited by surging. Therefore, complex and expensive concepts such as two-stage turbocharging has to be used for applications with high boost levels or large ranges of mass flow.

An alternative boosting method, based on a wave rotor approach, was developed also in Switzerland: the pressure wave supercharger (PWS), better known under its name Comprex [14]. The PWS has been used to supercharge diesel engines since the 1940s. At that time, the Brown Boveri Company (BBC) in Baden Switzerland started producing a PWS, the so-called Comprex. PWS applications were first developed in the 1940s as additional stages for locomotive gas turbines by BBC. The machine itself is therefore much more recent than the turbocharger. The PWS was used at former GM subsidiary Opel and by Mazda in 150,000 cars. However, some inherent problems of the PWS, especially regarding its cold-start behaviour, prevented the Comprex from having a commercial success.

However, high boost levels are becoming increasingly important for alternative fuels (such as hydrogen or methane) and alternative combustion concepts. Therefore, the Comprex may be a device which will bring benefits in future applications. Recently, the Comprex has been fundamentally redesigned by the Swiss company Antrova to overcome its known drawbacks [15] (Comprex is now a trademark of the Antrova AG subsidiary 3 prex AG, Stein am Rhein, Switzerland [16]). The main novelties are a completely water-cooled design, a split-rotor concept as well as flow-switching.

Antrova has provided two development stages of the Comprex. The first stage was initially designed for a passenger car application and used for initial tests (not reported here). Based on the results and experiences, Antrova designed a completely new Comprex especially for the F1C engine. This Comprex was produced using rapid prototyping methods and implemented, without any prior tests, on the test engine. Software adaptations of the engine control unit were also done in order to control the new degrees of freedom (Comprex speed, gas pocket valves, flow switching, wastegate). Further information on the design and background of this machine can be found in [17][18]. Fortunately, the design and production was excellent so that the Comprex performed excellently and survived all engine experiments without any damage.

The pressure wave supercharger that was used in this research is shown schematically in Figure 24. The low-pressure side consists of channels 1 and 4 whereas the high-pressure side consists of channels 2 and 3, respectively. A well understandable animation and further explanations can be found in [19].

In pressure wave superchargers the pressure energy is transferred from the exhaust to the intake side by bringing the two fluids into direct contact for a very short time in long, thin channels, the so-called rotor cells. Pressure wave machines use the physical principle that after two media of different pressure are brought into contact, the pressure equalization takes place faster than the mixing of the fluids. In case of the Comprex, mixing of exhaust gas and fresh air hardly takes place due to the different fluid densities.

It must be noted that the schematic shown in Figure 24 only shows half of the Comprex. In reality, what is shown in the schematic is only one "cycle" and the machine contains two cycles shifted by 180° around the circumference. There are two gas pocket valves which can be operated continually and independently from one another with a stepper motor for each valve.

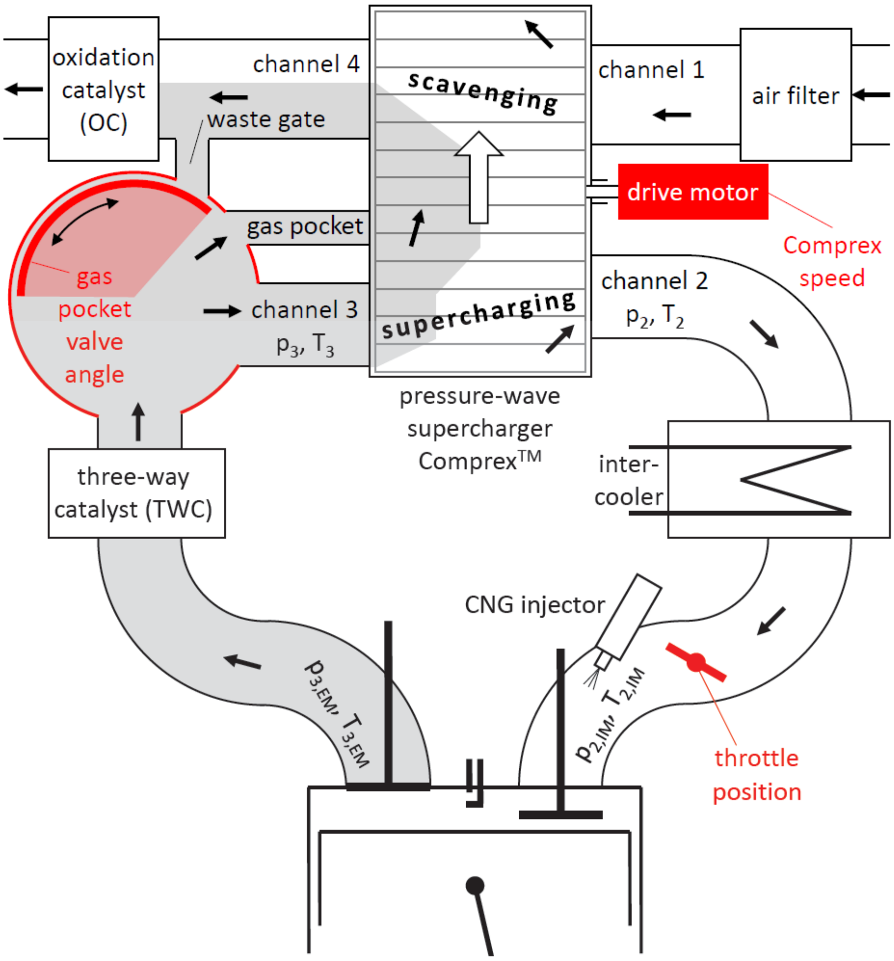

Figure 24: Schematic of the Comprex pressure wave supercharger. The description of the relevant pressures and temperatures is also indicated in the schematic.

For the load control of an engine equipped with this boosting device, there are four independent control inputs: rotor speed, throttle position, and both gas pocket valve angles.

Below naturally aspirated full load – as for turbocharged engines – the throttle is used to control the intake manifold pressure. When boost pressure is required, the gas pocket(s) must be closed in order to increase the back pressure and hence enable stronger pressure waves that will in turn increase the pressure in channel 2. The boost pressure can be controlled continually by changing the closed-off cross section of the gas pocket(s). At low engine speeds, one gas pocket valve is closed completely, forcing all the exhaust gas through half the machine, whereas at higher engine speeds both gas pocket valve angles are the same. At low engine loads, the gas pocket valve angle can also be chosen to open the wastegate cross section allowing the fluid to bypass the machine further reducing the backpressure. The load control is thus far similar to an engine equipped with sequential turbocharging.

The rotor speed of the Comprex, however, can be chosen freely and has an impact on the steady state operating conditions. In the following, this impact of the rotor speed is analysed in a low load and in a high load operating point.

4.10.1 Steady-state operation

For a high engine load the results are shown in Figure 25. At high engine loads, the resulting EGR rate remains low for all chosen rotor speeds. The trend for the rotor power is the same as for the low load operating point and it increases with increasing speed. There are, however, more significant changes to the exhaust gas backpressure and the temperature T_2. The boost pressure remains almost constant as it is controlled to keep the engine torque at a constant 400Nm (16.8bar brake mean effective pressure) for all measurements. The exhaust manifold backpressure on the other hand changes by approximately 0.1bar and has a minimum between a rotor speed of 10000 and 11000rpm. The temperature T_2 is lowest, where the scavenging of the rotor is highest. A reduced scavenging at a too low or too high rotor speed lead to a reduced cooling of the rotor which leads to an increase in T_2.

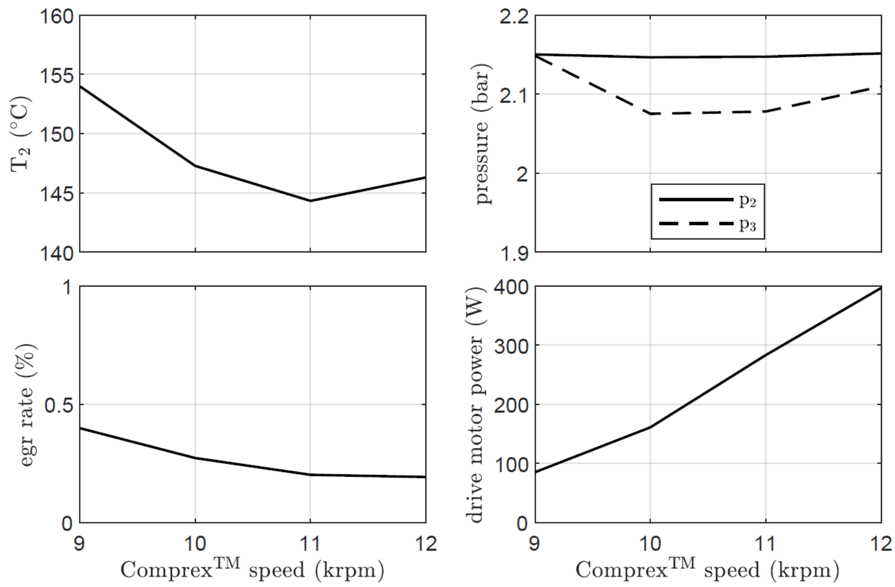

Figure 25: Variation of the rotor speed at 2250rpm and 400Nm, operation with both cycles.

We performed this analysis at 1250rpm, 2250rpm and 3250rpm and several engine loads and chose the following rotor speed map, which we interpolated/extrapolated for different engine speeds and extrapolated for higher engine loads. We used this speed map, which is shown in Figure 26, for all following measurements in the entire operation map, at full loads, part load, for transient operation as well as for the analysis of the exhaust gas aftertreatment system.

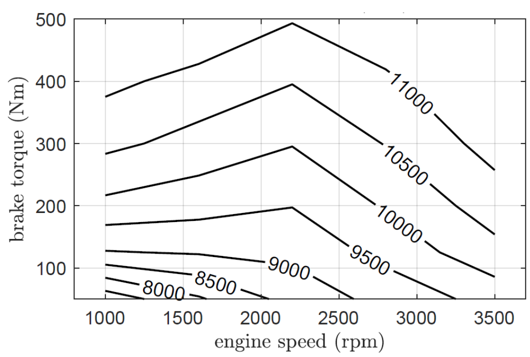

Figure 26: Comprex speed map that was used for the experimental analysis.

The full load operation is analysed here in all combinations both boosting devices and both camshafts. For convenience, the configurations are abbreviated as described in Table 2.

Table 2: Abbreviations used for the different engine configurations

Boosting device	Camshaft	Abbreviation
Comprex	Conventional	CXC
Turbocharger	Conventional	TCC
Comprex	Miller	CXM
Turbocharger	Miller	TCM

The main limitations that had to be respected are:

- Maximum cylinder head temperature 250°C
- Latest centre of combustion 20°CA after top dead centre
- Light knocking should occur in maximum in 4% of the cycles

The centre of combustion and the knock criterion are chosen somewhat arbitrarily. This is done in order to not stress the engine too much (knock criterion) as this is an engine for light duty applications that must have a high durability and to ensure comparability between the different measurements (COC).

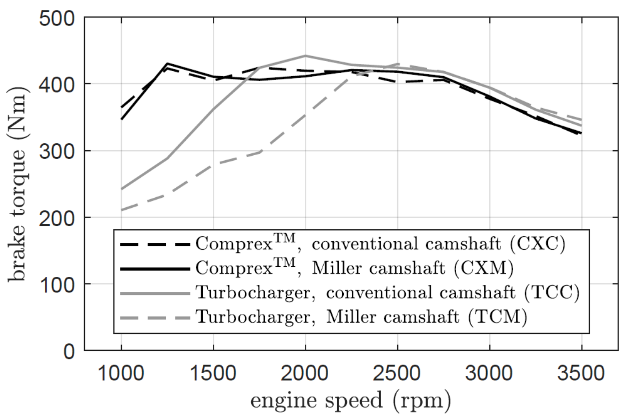

Figure 27: Full load brake torque results with different charging systems and different camshafts.

Figure 27 shows the maximum brake torque that was achieved with the configurations CXC, CXM, TCC, and TCM, respectively. At engine speeds above 2500rpm the results are similar for all configurations. Both configurations of the turbocharged engines lead to results that are practically identical. The CXM configuration results in a slightly lower torque because of the slightly higher temperature level of the charged fresh air of the Comprex compared with the turbocharger (which could easily be recovered by an adapter intercooler). A torque larger than 400Nm is possible up to 2750rpm for all configurations and this is where the maximum cylinder head temperature is first reached. For higher engine speeds, this temperature is also the limiting factor.

The engine power output remains constant for each configuration at higher engine speeds and the torque reduces accordingly. For the turbocharged configurations at low engine speeds the Miller camshaft leads to a significant reduction in low-end torque. Despite the fact that the wastegate is fully closed up to an engine speed of 2250rpm, only at that engine speed a torque larger than 400Nm is first achieved due to a lack of boost pressure at lower engine speeds.

While the turbocharged engine with the conventional camshaft surpasses 400Nm at 1750rpm, it is impressively outperformed by the Comprex, even if Miller valve timing is used. In the CXM configuration, 430Nm are reached at an engine speed of 1250rpm and up to engine speeds of 1750rpm the Comprex is operated with one cycle. In this configuration the load control actuator is only in its saturation at 1000rpm, i.e. there would still be potential to increase the boost pressure at all other engine speeds. Further data of the most important temperatures and pressures are compared in Figure 28.

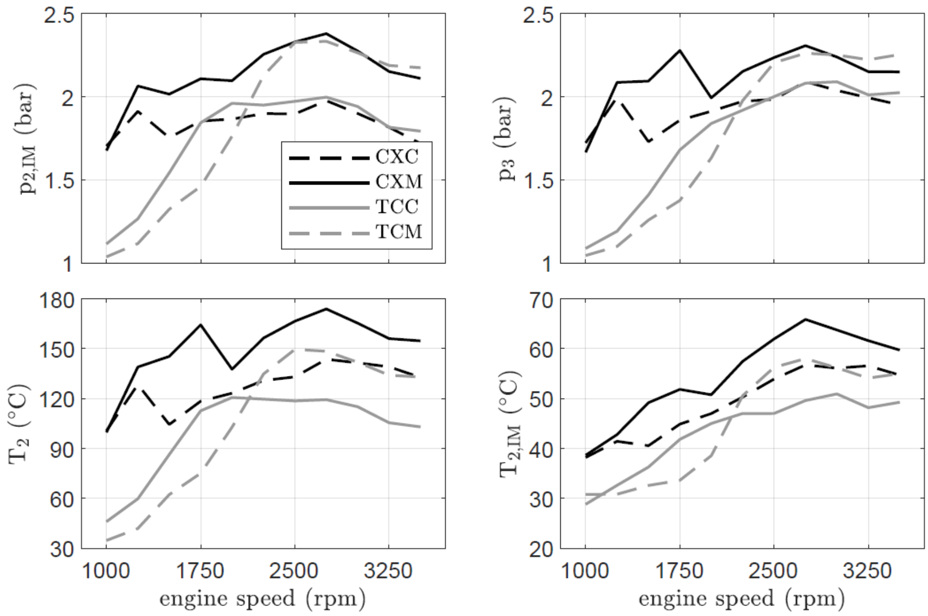

Figure 28: Pressures and temperatures during full load operation.

The upper plots of Figure 28 show the intake manifold and the exhaust manifold pressure, respectively. Obviously, due to the early valve closing in Miller configuration the pressure levels in case of the CXM concept is much higher. At high engine speeds, when a high brake torque can also be achieved with the TCM configuration, the boost pressure level between the two Miller configurations is similar. At low engine speeds, however, the difference is even larger, since a high torque output can only be reached with the Comprex/Miller configuration.

For the TCC concept the boost pressure is higher than the exhaust gas backpressure up to an engine speed of 2250rpm whereas for the CXM configuration this is the case from 2000rpm to 3250rpm. The bottom plots of the temperatures show that in the engine speed range where the boost pressure for both Miller concepts is similar, the temperature after compression T2 and the intake manifold temperature $T_{2,IM}$ are both higher when the Comprex is used. To some extent the difference may be reduced by optimizing the Comprex rotor speed for all engine speeds. However, in general it can be stated that a larger intercooler may be required to compensate for the slightly higher T_2 level of the Comprex, a measure which can easily be done.

To quantify the fuel savings potential that results from the use of a Miller camshaft measurements are taken in the entire operating range in addition to the full load measurements shown in the previous Subsection. Figure 29 shows the part load results for the configurations Comprex and Miller camshaft (CXM) and Turbocharger and conventional camshaft (TCC), respectively, for an engine speed of 2200rpm where the load was increased from 50Nm to 350Nm in steps of 75Nm. For the CXM concept, the power required to drive the Comprex has been taken into account. The engine speed of 2200rpm was chosen since low/medium speeds are more relevant for daily operation and at lower engine speeds the maximum torque of the turbocharged engine was too low for a comparison over the entire load range.

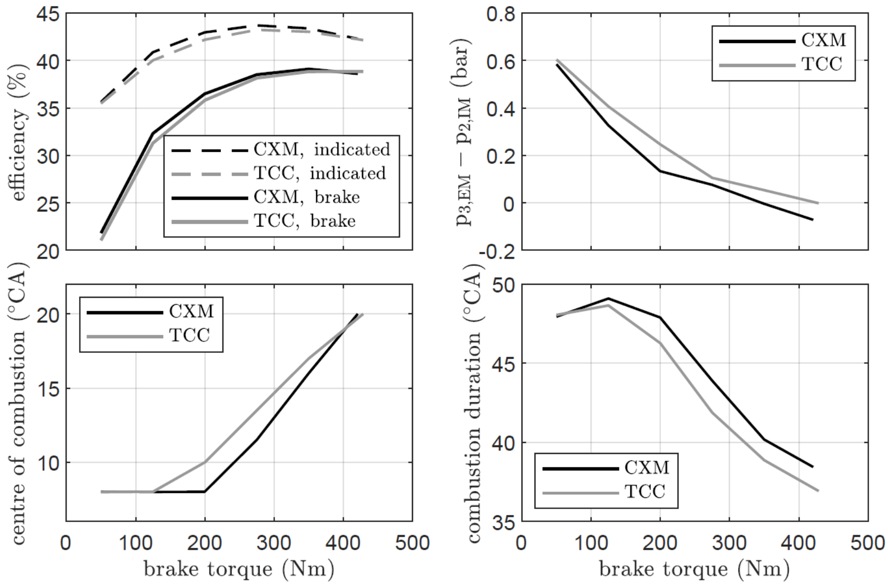

Figure 29: Part load results of efficiency, gas exchange and combustion for an engine speed of 2200rpm.

The indicated efficiency and brake efficiency that were reached with both configurations are shown in the top left subplot. Except for the highest load point there is always an advantage for the CXM configuration in both indicated and brake efficiency.

One reason for this improvement is the pressure difference between the exhaust gas backpressure $p_{3,EM}$ and the intake manifold pressure $p_{2,IM}$, which is shown in the top right subplot. In the entire load range, the pressure difference is favourable in case of the CXM configuration.

The two bottom plots of Figure 29 show the centre of combustion and the combustion duration, respectively. While the combustion duration increases slightly in case of the CXM concept, the centre of combustion is closer the brake-optimal value of 8◦CA except at the highest load point, where in both cases 20°CA is used. The numerical values for the improvements in brake efficiency that are achieved with the CXM concept are shown in the table below.

Brake torque	50Nm	125Nm	200Nm	275Nm	350Nm
Relative improvement	3.63%	3.26%	1.87%	0.94%	0.69%

Additionally to these measurements at 2200rpm, measurements for the operating maps were taken at 1000rpm, 1600rpm, 2800rpm, and 3500rpm. The trends, however, that are shown here are the same for all other engine speeds as well. Except for low engine speeds, where the CXM concept reaches much higher brake torque values, it is only the highest load point where the CXM concept has a lower efficiency than the TCC concept. The Miller concept is advantageous at low and medium loads and is enabled by using the Comprex charger.

Due to the way the Comprex is designed, an engine braking capability is facilitated without the use of additional components such as an exhaust flap. By closing the gas pocket valve(s) successively, the pressure in the exhaust manifold can be increased which in turn results in a very low (negative) mean indicated pressure.

The engine braking capability is limited by the maximum permissible backpressure of the exhaust system. This pressure limitation results either from the preload of the exhaust valve springs (the valves may not open unintentionally) or from other pressure limitations of exhaust components (e.g. expansion joint).

For these measurements, the engine was operated at 50Nm at three different engine speeds and then the fuel injection was cut off. The throttle plate was kept at the same position and the gas pocket valve(s) were closed successively to increase the exhaust backpressure. Measurements were taken up to a torque <-100Nm for engine each speed.

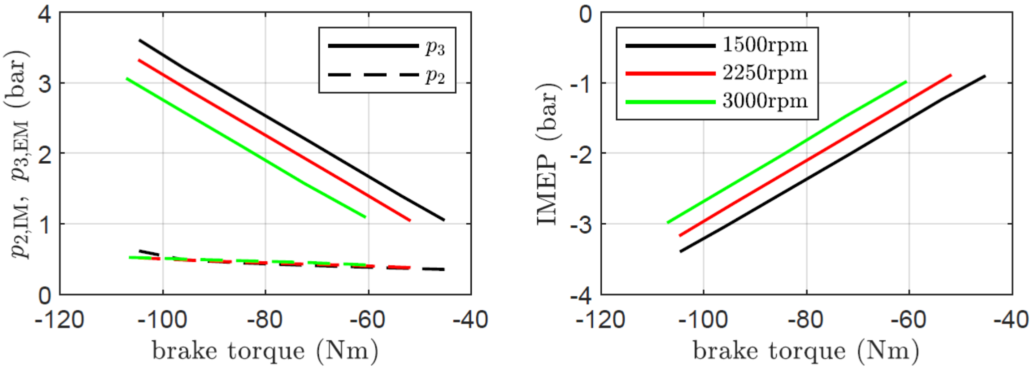

Figure 30: Engine braking with the Comprex. The different colours represent different engine speeds. In the left subplot, the solid lines show the exhaust gas pressure $p_{3,EM}$ and the dashed lines show the intake manifold pressure $p_{2,IM}$.

Figure 30 shows the results of these measurement series. The left plot shows that there is a linear correlation between the backpressure $p_{3,EM}$ and the brake torque. Increasing the backpressure also reduces the engine mass flow, which is why the intake manifold pressure $p_{2,IM}$ slightly increases using the constant throttle position. The right plot shows that these two linearly increasing pressures also result in a linearly decreasing indicated mean effective pressure (IMEP) for each engine speed. These IMEP-traces are only offset by the mechanical friction of the engine. During all measurement series, even after several minutes of motored operation, the exhaust gas temperature at the pre-cat never fell below 180°C. This can help to reduce the wear of the mechanical brakes and also to keep the exhaust aftertreatment warm during longer phases of motored operation.

Simulation results of driving cycles show that using this engine braking capability, the use of friction brakes can be reduced by 64%…68% depending on the vehicle and driving cycle.

4.10.2 Transient operation

Besides steady state operation and quasi-steady-state driving cycles, transient operation is analysed in this section. In general, the use of a Miller camshaft is detrimental to transient operation for two reasons. On one hand, a lower mass flow results from the early intake valve closing at wide-open throttle condition and on the other hand a higher boost pressure must be reached for the same torque output. However, one property of a Comprex is that a fast increase of the boost pressure is possible and another property that was already shown in this paper is that it is easily possible to reached a high boost pressure. Therefore, to quantify this somewhat unfair comparison (with disadvantage for the Comprex) between the Comprex supercharger with a Miller camshaft and the turbocharger with a conventional camshaft, load steps were carried out. In order to assess the transient performance over a wide engine speed range, this was done at 1250rpm, 1750rpm, 2250rpm, and 3250rpm and the resulting torque trajectories are shown in Figure 31.

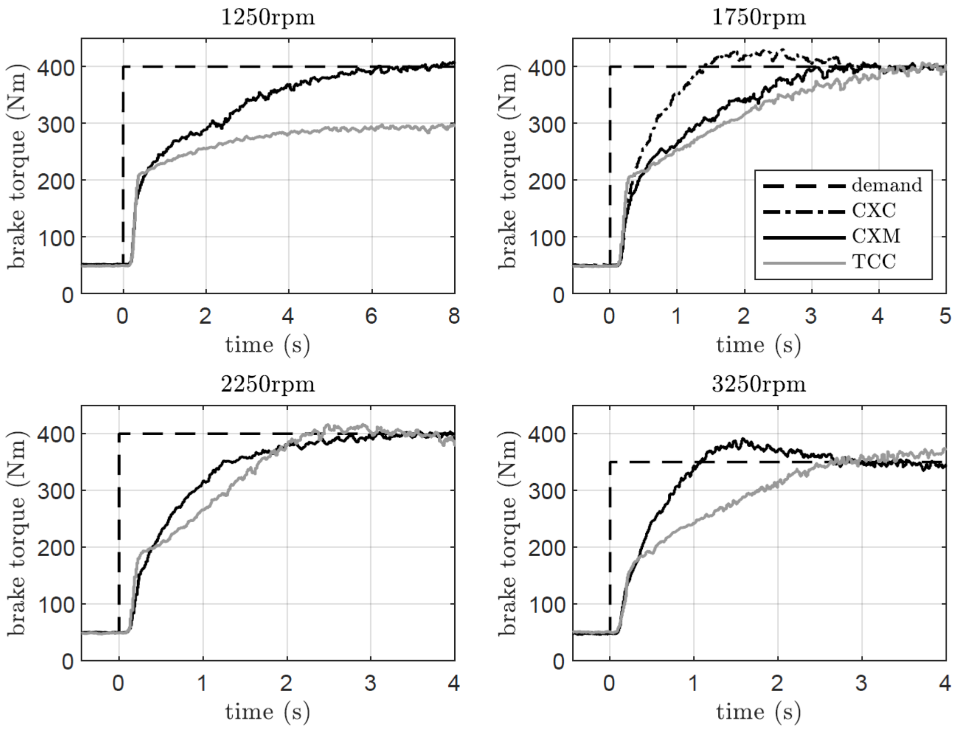

Figure 31: Load steps at several engine speeds using two (three) different engine concepts: Comprex with Miller camshaft (CXM), Comprex with conventional camshaft (CXC) and turbocharger with conventional camshaft (TCC). Notice the different scaling of the x-axes.

Table 3 summarizes the times it takes to reach 80% and 90%, respectively, of the desired torque and also the difference between the two concepts.

Table 3: Key numbers for transient load step responses

Engine speed	t80/t90 CXM (CXC)	t80/t90 TCC	Relative duration
1250rpm	2.66s/3.79s	–/–	–/–
1750rpm	1.61s/2.28s (0.79s/1.10s)	2.05s/2.84s	+27%/+24% (+159%/+158%)
2250rpm	1.07s/1.46s	1.42s/1.78s	+33%/+22%
3250rpm	0.70s/0.84s	1.46s/2.01s	+110%/+140%

At 1250rpm, the difference in the torque trajectories is the largest because the turbocharged engine is only able to reach <300Nm while the Comprex provides enough boost pressure for >400Nm. At this engine speed it takes less than 3 seconds to reach 85% of the desired torque. During the load step the Comprex speed increases from 7500rpm to 11000rpm which requires approximately five seconds. This leads to significant differences between the steady state and the instantaneous Comprex speed of up to 2300rpm. However, as shown with the Comprex speed variations, this simply leads to an increased backpressure and increased temperature for several seconds, which is not a problem.

At an engine speed of 1750rpm and 2250rpm, the response of the turbocharged engine is almost as fast as that of the Comprex. A load step was also carried out with the Comprex and the conventional camshaft at 1750rpm to assess how significant the disadvantage due to the use of the Miller camshaft is and also to show the potential of the Comprex supercharger. As noted in Table 3, in this case the time for the torque response of the turbocharged engine is approximately 2.5times as long as for the Comprex. At 3250rpm, the torque response of the Comprex is again significantly faster than that of the turbocharged engine. However, the reason in this case is the pneumatic wastegate actuator that is used for the turbocharged engine which is rather slow. At the other engine speeds, this is not relevant, since the time for those torque build-ups is long compared to the time it takes to close the wastegate. At high engine speeds, then the torque increase is faster anyway, the dynamic of the wastegate becomes relevant.

These results show that the transient behaviour of the engine equipped with the Comprex supercharger is better than that of its turbocharged counterpart, even if a Miller camshaft is used in combination with the Comprex. When the same camshaft is used for both charging devices, the advantage of the Comprex is larger.

4.10.3 Exhaust gas aftertreatment with a Comprex

Regarding the exhaust aftertreatment system, there are two fundamental differences when a Comprex concept is used. On one hand, the TWC is placed upstream of the boosting device in the high pressure part of the exhaust system. On the other hand, the OC operates under lean conditions, even if there are stoichiometric conditions at the TWC due to the scavenging of fresh air to the exhaust side. The TWC that is used for this comparison is the same for both concepts and it is a series production component. The tested turbocharger aftertreatment setup consists of series production components for both catalytic converters (two stages TWC) and therefore representative of real life scenarios.

The TWC inlet temperatures and emissions before/after each catalytic converter are measured at various engine operating points across the complete engine map. Additionally, the cold start behaviour is recorded while the engine warms up from stand still at a low load operating point (1000rpm, 50Nm and a centre of combustion of 8◦CA after top dead centre). These measurements are carried out for both concepts under the same conditions.

The first stage/upstream TWC inlet gas temperature at various operating points are shown in Figure 32a) for both conventional turbocharger setup (temperatures listed in brackets) and Comprex setup (temperature listed without brackets). Compared to the conventional turbocharger setup, the TWC in the Comprex aftertreatment layout is subjected to exhaust gases of 25 to 90◦C higher temperature, due to the catalyst mounting location upstream of the Comprex. The higher inlet temperature for the catalyst means better conversion rates in the TWC under the same exhaust gas compositions. TWC in Comprex setup is mounted at the high pressure side of the charging device, which means that the residence time of hot exhaust gas is longer compared to conventional setups. The longer residence time, together with the higher temperature affects the catalyst warm up behaviour.

A significantly faster increase of TWC outlet temperature for the Comprex setup (top plot Figure 32b)) is observed. The CO conversion rate of the first stage/upstream TWC during the cold start are plotted in the bottom plot of Figure 32b). With the Comprex setup, the time to reach 50% conversion of CO is 14.0 seconds, while this time increases to 91.7 seconds with the turbocharger setup (vertical line in Figure 32b). The Comprex setup therefore shortens the lightoff time by a factor of 6.

The authors are aware, that this is not a state-of-the-art catalyst warmup strategy. Typically, the centre of combustion is very late during this phase and the fuel enery is used to generate heat in the warmup phase. However, we quantified the difference in this simplified way in order to point out the significant difference in thermal inertia which is crucial for a fast catalyst warum regardless of the strategy. A strategy with late centre of combustion for the Comprex concepts would lead to a very fast catalyst warmup and would only be required for a very short period of time and therefore lead to a minimal fuel penalty. As in real life scenario considerable emissions typically result from the cold start phase, the decrease of light-off time with the Comprex setup is a significant advantage in terms of total emissions.

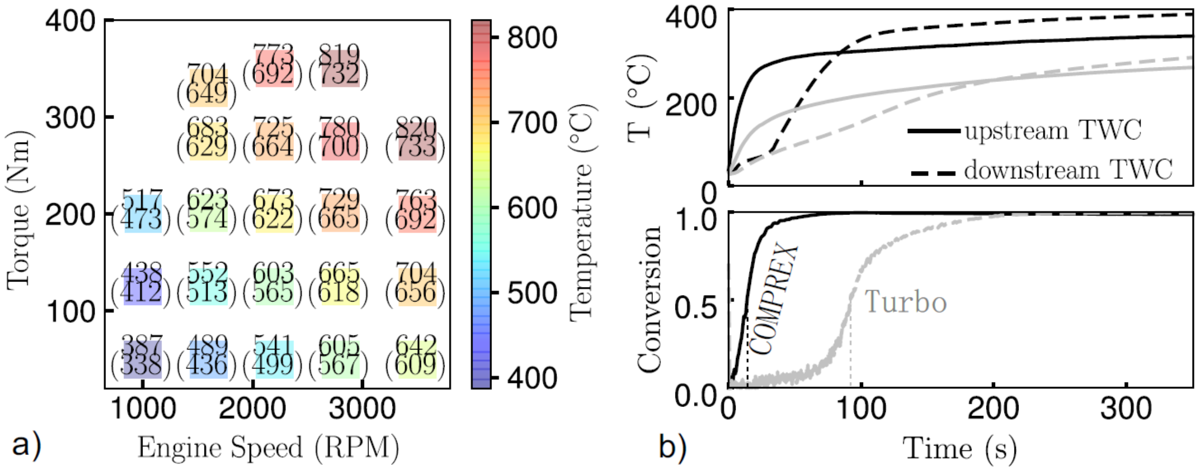

Figure 32: a) steady state temperature upstream of the precat for the Comprex and the turbocharger in brackets. At low engine loads the centre of combustion was set to 8◦CA after top dead centre in all cases.

b) Temperature (top) and CO conversion rate (bottom) evolution during cold start at 1000rpm and 50Nm, centre of combustion 8◦CA after top dead centre start for Comprex setup (black) and turbocharger setup (grey). A Comprex speed of 4000rpm was used for this cold start measurement.

The potential of pollutant conversion of the TWC in the Comprex Setup system is further studied with steady state and dithering measurements under several selected operating conditions (tabulated in Table 4). For dithering measurements, the air-to-fuel-ratio oscillates around $\lambda = 1$ with high frequencies. The conversion rates of major species under steady and dithering conditions are plotted in Figure 33a). It is clear that in combination with appropriate dithering strategies, the THC conversion rate stays above 65%, CO conversion rate above 70%, and the NOx is almost 100% converted. Compared to steady operation, dithering strongly enhances THC conversion and also promotes CO conversion, while the engine out raw emission for steady and dithering operation is rather similar (Figure 33b)).

The dithering operation, however, leads to high H2 concentration after the TWC (Figure 33c)), most likely due to the activation of steam reforming over dithering [20].

Table 4: Operating conditions for aftertreatment experiments

Engine speed	Brake torque	Temperature inlet TWC	Temperature inlet OC
1000rpm	50Nm	375°C	151°C
1600rpm	50Nm	477°C	198°C
1600rpm	100Nm	517°C	232°C
2200rpm	97Nm	586°C	297°C
2800rpm	80Nm	625°C	347°C
2800rpm	117Nm	660°C	397°C

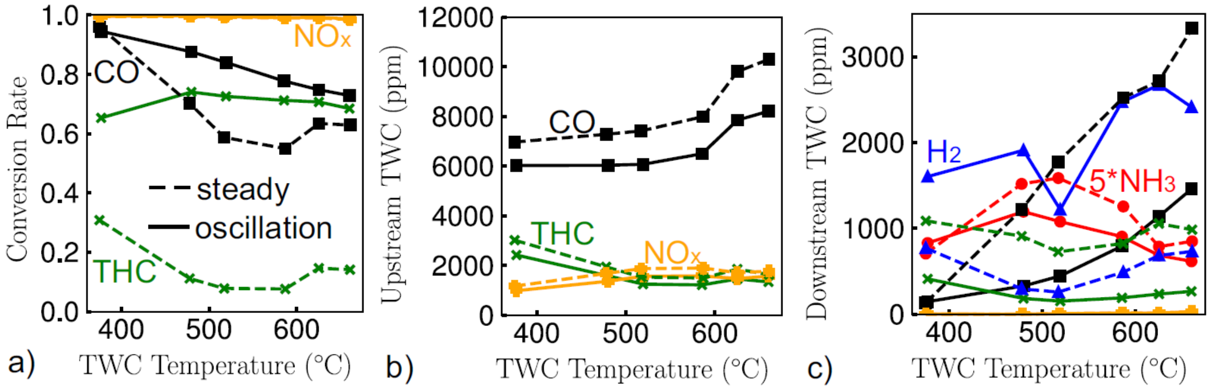

Figure 33: a) Conversion rates of NOx, CO, THC in upstream TWC

b) Concentration of CO, THC, NOx upstream of TWC

c) Concentration of CO, THC, NOx downstream of TWC during steady and dithering operations.

As described in the previous section, the special design of Comprex charging system induces mixture of fresh air and exhaust gas in channel 4. The remaining CO, dithering induced excess H2 and NH3 can be removed by oxidation reactions with the additional oxygen in an oxidation catalyst downstream of channel 4. Methane (main content of the THC in the exhaust) is notoriously difficult to be oxidized under lean conditions [21], and is therefore left out of the OC analysis. Figure 34a) plots the conversion rates of H2, CO and NH3 at the six operating points tabulated in Table 1. The OC inlet temperature is higher than 150◦C even at the lowest load point (1000Nm, 50Nm), which results in near 100% conversion of CO and more than 80% conversion of H2 under dithering operation. NH3 is hardly converted at this low temperature. Unsurprisingly, the oxidation conversion increases over temperature. NH3 starts to be oxidized at above 200◦C and reaches more than 80% conversion rate at around 230◦C with dithering. The same dithering strategy is also implemented on the turbocharger aftertreatment setup at the same engine operating conditions, which consists of a second stage TWC instead of the oxidation catalyst in Comprex setup. Oxygen is completely consumed in the first stage of TWC (not shown). Without additional oxygen, oxidation pathways of the remaining pollutants are blocked.

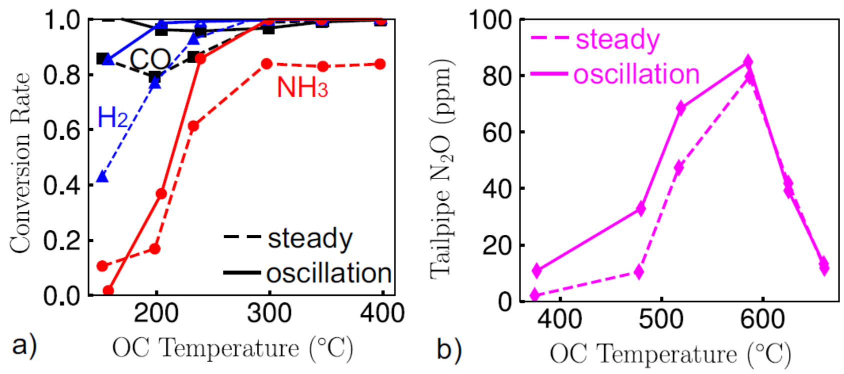

Figure 34: a) Conversion rates of H2, CO, NH3 in oxidation catalyst b) Concentration of N2O downstream of TWC during steady and dithering operations.

The oxidation catalyst used on the Comprex system is a Pt catalyst, typically used in Diesel applications. Even though Pt only catalyst is excellent in oxidizing CO, the oxidation of NH3 with Pt results in undesired products. Figure 34b) plots N2O concentration at the outlet of the OC and shows that a noticeable amount of N2O is formed during NH3 oxidation. The results suggests that further investigations on alternative catalyst formation are needed to increase the selectivity toward N2 during

NH3 oxidation. Nevertheless, the unique layout of ATS system enabled by the Comprex setup exhibits various advantages toward a traditional turbocharger setup. In combination with targeted dithering strategy, the aftertreatment system delivers high conversion rate toward THC, NOx and CO with the potential benefits of oxidizing remaining NH3, H2, CO with additional oxidation catalyst downstream.

4.11 Water injection results

As in all configurations the cylinder head temperature is the factor that limits the maximum power output, a temperature reducing measure is presented here. The injection of water is a known measure to reduce the temperature level in an internal combustion engine and also to reduce the knock tendency. The engine was equipped with port fuel water injectors to test the effects of water injection on the engine full load. The injectors were designed by means of 3D CFD simulation by Nostrum Energy (Ann Arbor, MI, USA). A special feature of the Nostrum injectors is the colliding jet technology which enables very small droplets and, with a proper spray targeting, low wall wetting. Figure 35 shows some CFD results of the spray targeting design. The injector is located in the intake manifold and the spray targeting is such that the walls of the intake runner are penetrated as little as possible and the water arrives in the combustion chamber with a small droplet size.

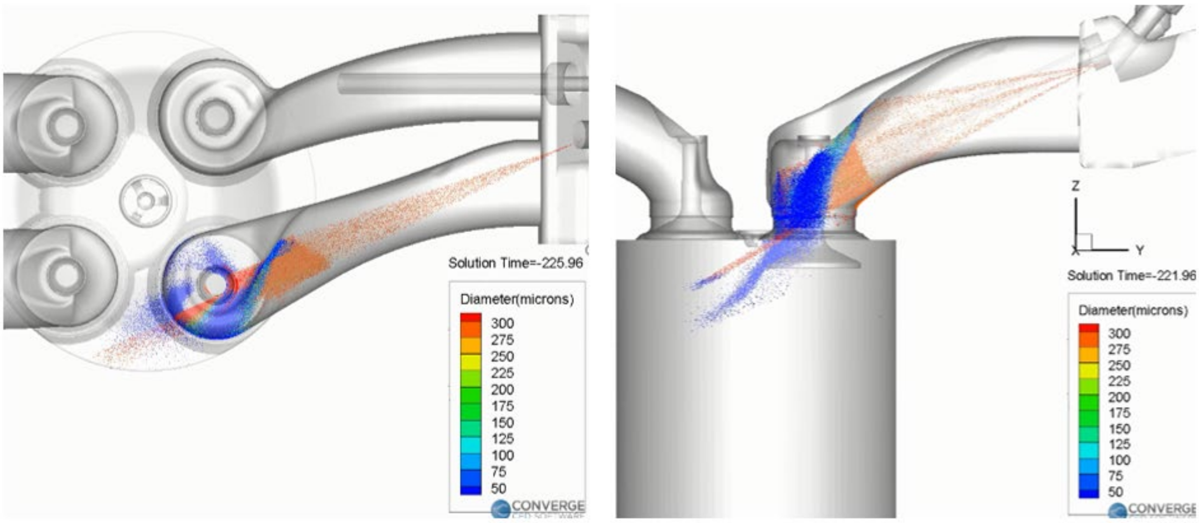

Figure 35: top view (left) and side view (right) of the CFD design of the port water injectors by Nostrum Energy.

In a measurement series at 3000rpm/300Nm, different water/fuel mass ratios were used to analyse the impacts on the combustion. The brake torque was kept constant, while the water/fuel ratio was increased from 0% to 80%. The water was injected at a pressure 5bar higher than the intake manifold pressure and the start of injection was right after the intake valve opening angle. The centre of combustion was corrected for each water/fuel ratio, such that the engine operation was at the onset of knock in each measurement.

Figure 36 shows the effect of the water injection on the combustion parameters. The upper left plot shows that with increasing water/fuel ratio, the centre of combustion can be advanced. This is due to the dilution of the mixture with water vapour which slows down the combustion and the cooling effect of the water evaporation. The upper right plot shows the inflammation duration, i.e. the duration from the ignition angle until 5% of the mixture are combusted. The flame development phase takes significantly longer when a higher water/fuel ratio is used. The bottom left plots shows the heat release rate for five operating conditions and the earlier combustion start can be seen in the graph. The figure also shows that the peak heat release rate is lower and the combustion duration increases when more water is present during the combustion. The result of these effects on the combustion is a change in the brake efficiency, which peaks at a water/fuel ratio of 40% and is approximately 0.4%-points higher (i.e. the fuel consumption is about 1% lower) compared to the operation with no water injection. For higher water/fuel ratios the combustion duration becomes less favourable and the efficiency reduces again despite the fact that the centre of combustion is closer to 8◦CA.

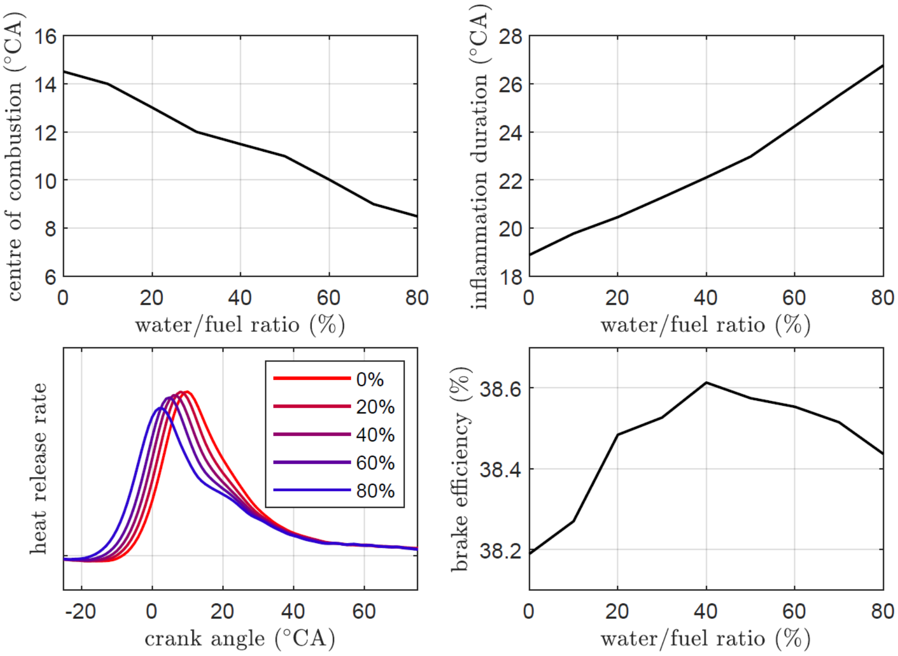

Figure 36: Effects of water injection on the combustion at an engine speed of 3000rpm and a brake

During these measurements, the coefficient of variance of the indicated mean effective pressure reduced from 1.53% without the injection of water to 0.87% at a water/fuel ratio of 80%.

Figure 37 shows the main influence of water injection on relevant temperatures and raw emissions. The upper left plot shows that the exhaust gas temperature T_3, which is measured at the entry of the turbine housing, reduces significantly with an increased water/fuel ratio. The cylinder head temperature, which is measured between the exhaust valves, also reduces when a higher water/fuel ratio is used. The bottom left plot shows that the reduction in temperature is accompanied by a reduction in the NO_x raw emissions. However, due to a more incomplete combustion, the raw emissions of hydrocarbons increase.

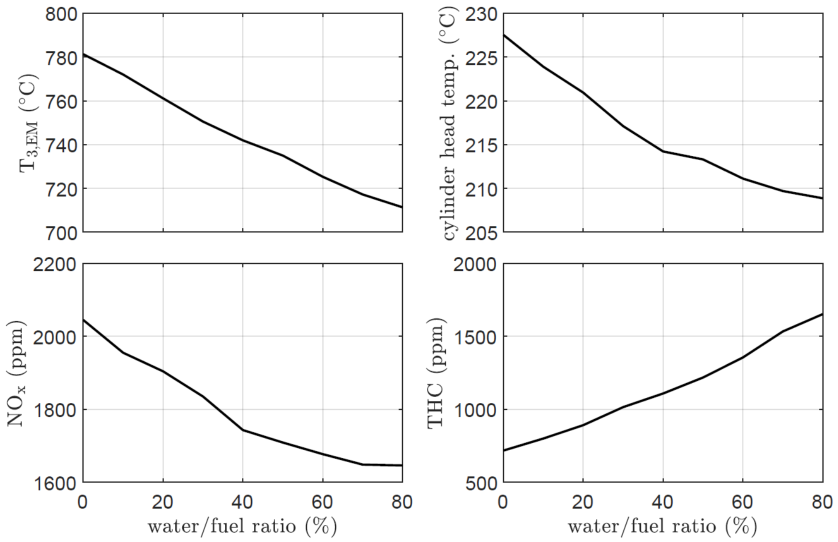

Figure 37: Effects of water injection on the relevant temperatures and engine-out emissions at an engine speed of 3000rpm and a brake torque of 300Nm.

As the cylinder head temperature is the limiting parameter for this particular engine regarding the maximum power output, this shows that there is a potential to increase the power output. However, it is also true in general, that CNG engines which sometimes are derivates from Diesel engines suffer from limits in the operating temperatures and water injection is an effective measure to reduce/avoid this problem.

To quantify the possible increase in the engine power output, full load measurements were made at 2750rpm for the TCC and the CXC concept with water fuel ratios of 0%, 25% and 50%. The results of these measurements are shown in Figure 38. The centre of combustion remains at the chosen limit of 20◦CA for all measurements and the intake manifold pressure is increased until the onset of knock is reached.

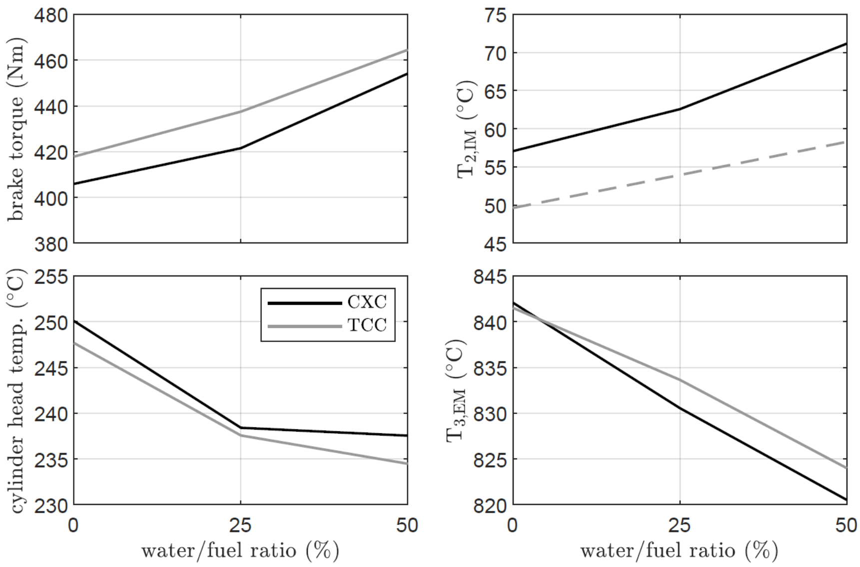

Figure 38: Effects of water injection on the full load at a given centre of combustion of 20◦CA at an engine speed of 2750rpm.

The upper left plot shows that the brake torque can be increased by 48Nm and 47Nm for the CXC and the TCC concept, respectively. The increased boost pressures lead to increasing temperatures on the intake side as shown in the upper right plot. Despite this increase, the exhaust gas temperature as well as the cylinder head temperature both reduce as shown in the bottom plots.

These results show that an increase in the peak engine power is possible using water injection for both concepts. Just as in the previous section, the turbocharged engine has some advantage due to the lower intake manifold temperatures. It must be noted that allowing a later centre of combustion and/or increasing the water/fuel ratio would leave room for a further increase of the power output until the maximum cylinder head temperature is reached once again.

Apart from these conceptual comparisons at one engine speed, also comparisons at all engine speeds in the turbocharged configuration and at low engine speeds with Comprex supercharger are presented briefly here

Figure 39 shows the full load results at all engine speeds when different rates of water injection are used with the turbocharged engine. At low engine speeds, there is always a lack of boost pressure and the water injection does not help to achieve higher loads. However, at medium and high engine speeds – where more boost pressure would be possible and the engine is knock/or temperature limited – the torque can be increased significantly. The plot on the right hand side shows that for engine speeds greater/equal to 2750rpm the engine operation is limited by the maximum cylinder head temperature of 250°C when no water injection is used (red lines). Using a water/fuel ratio of 25% (blue lines), this temperature is first reached at 3250rpm and the maximum power/torque at that engine speed is increased by 12%. Using a water/fuel ratio of 50% (green lines), measurements were only taken up to an engine speed of 3000rpm. The reason is that the fuel lass flow was at its limit and the full potential of engine/water injection could not be reached due to this test bench limitation. Nevertheless, at 3000rpm an increase of 16% could already be shown.

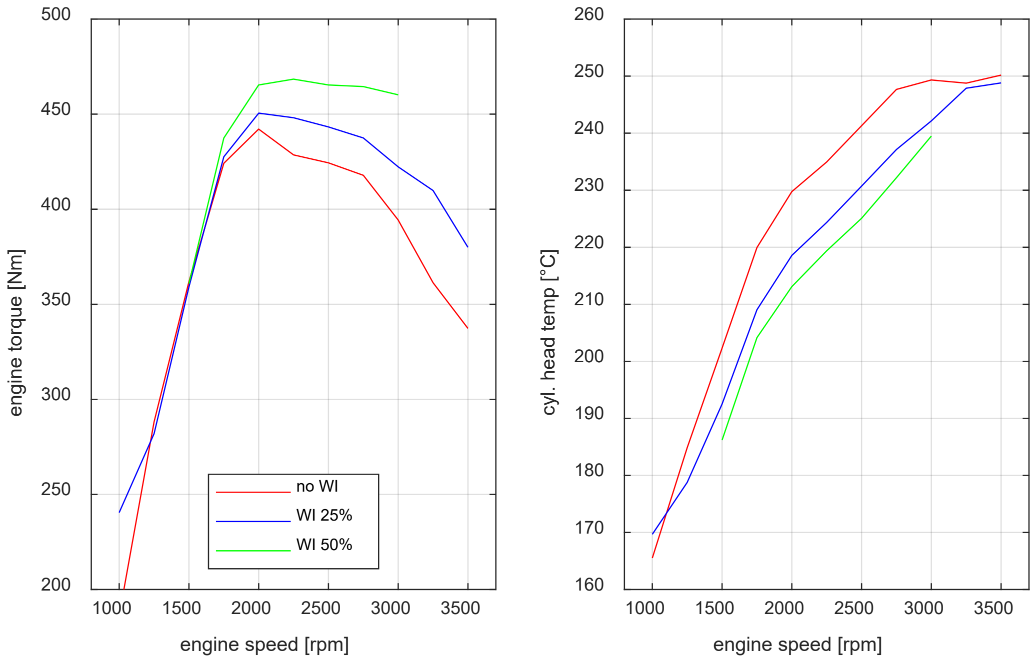

Figure 39: Full load with turbocharger. COC = 20°CA and different rates of water injection.

For low engine speeds, measurements at 1250rpm and high load conditions were carried out with the Comprex supercharger. Figure 40 shows that the trends are essentially the same as previously described. For each load, the centre of combustion can be advanced when the water injection rate increases. The brake efficiency also increases up to a water/fuel ratio of 40% or 60%. The higher the water/fuel ratio, the longer the combustion and the lower the exhaust gas temperature. The improvements in brake efficiency in these measurements ranges from 0.25%-0.4%. In literature, significant efficiency improvements in the low-end-torque operating regime of up to 10% are sometimes reported. With the given hardware, this is not possible mainly due to two reasons. The first reason is the brake torque level. This engine at 480Nm operates at a brake mean effective pressure of slightly over 20bar. The engines were these significant improvements are reported operate at significantly higher BMEP of 25…30bar. This would correspond to 595Nm and 714Nm, respectively, and is not possible with the given hardware. The other reason is the fuel. The reported results are typically obtained using gasoline engines. As CNG is significantly more knock resistant compared to any gasoline, problems with knocking combustion are much lower. As the bottom right plot of Figure 40 shows, regardless of the water/fuel-ratio the brake efficiency at 480Nm is only slightly lower than the corresponding maximum value, despite the fact that a piston with a very high compression ratio of 16.5 was used for these measurements.

These results show that using a COC lather than 20°CA the engine could reach 480Nm with the Comprex Supercharger at low engine speeds. At that speed, the cylinder head temperature is never the limiting factor. However, this is only possible with the Comprex supercharger and in that case the maximum cylinder head temperature of 250°C is reached already at 2250rpm leading to a somewhat strangely shaped maximum torque curve. As a recommendation, a brake torque of 425Nm could be used. With the Comprex supercharger, this is possible already at <1250rpm up to 2750rpm and with the turbocharger this is possible from <1750rpm up to 2750rpm. This corresponds to an increase of 21.4% compared to the 350Nm of torque output in the base-engine setup and hence exceeds the project goal of a 20% torque increase.

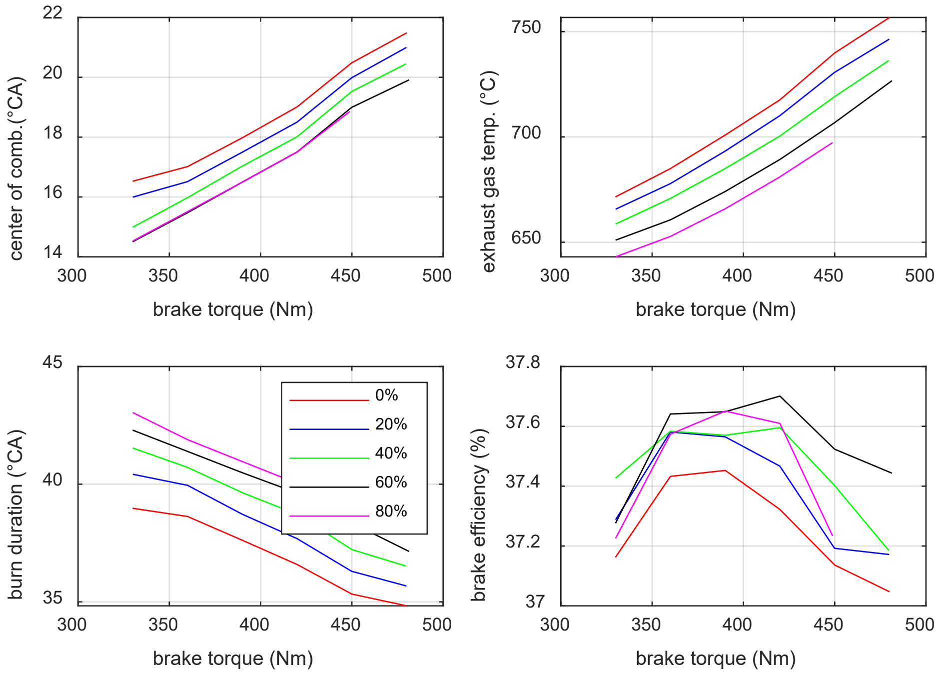

Figure 40: Full load with Comprex supercharger at 1250rpm.and different rates of water injection

These results also show that using water injection (in combination with either boosting device) and a later COC could lead to an increase of the power output greater that the 16% increase shown here in

Figure 39. Please note that the 50% water injection result at 3000rpm already corresponds to a power output of 144.5kW, which is an increase of 44.5% compared to the 100kW base-engine. The results without water injection correspond to an increase of 23% compared to the 100kW base-engine. Therefore, even without water injection and only due to the use of the split-core cylinder head the project goal of a 20% increase in power output could be achieved. A further increase in power, however, can only be reached with better cooling, for which water injection is suited well.

4.12 Fuel consumption, hybridization and drivability

To analyse the fuel consumption benefit in driving cycles, simulations based on the test bench measurement data were carried out. The driving cycles were simulated with a temporal resolution of one second using a quasi-steady-state framework and all engines are equipped with a stop-start system. The engine cold start and transient engine operation are not included in this framework, however, this type of simulation allows for a comparison of different concepts. The gearshift strategy is optimised by the simulation framework, which is based on dynamic programming. In case a simulation is run for a hybrid vehicle, the gearshift strategy as well as the operating strategy for the electric machine are both optimised by the simulation framework.

The main vehicle parameters, that were used in the simulations, are summarized in Table 5. As a driving pattern, the realistic WLTP procedure is used. The driving cycles that are used in the WLTP depend on the power-to-weight ratio of the particular combination of engine and vehicle. Since this engine is used in many different light commercial vehicles that have a maximum weight ranging from 3500kg up to 7200kg, it is relevant to assess the fuel consumption for vehicles of all masses.

Table 5: Main parameters of the simulated vehicles

Vehicle masses	2750kg/5000kg/7000kg
Rolling resistance coefficient	0.01(-)
Drag coefficient	0.5(-)
Frontal area	5.4m^2
Wheel rolling radius	0.35m
Gearbox gear ratios 1-8	5, 3.2, 2.143, 1.72, 1.314, 1, 0.822, 0.64(-)
Final drive gear ratio	3.5(-)

Therefore, simulations have been carried out for vehicle weights of 2750kg, 5000kg, and 7000kg which leads to the use of all three of the WLTP's driving cycles that are shown in Figure 41.

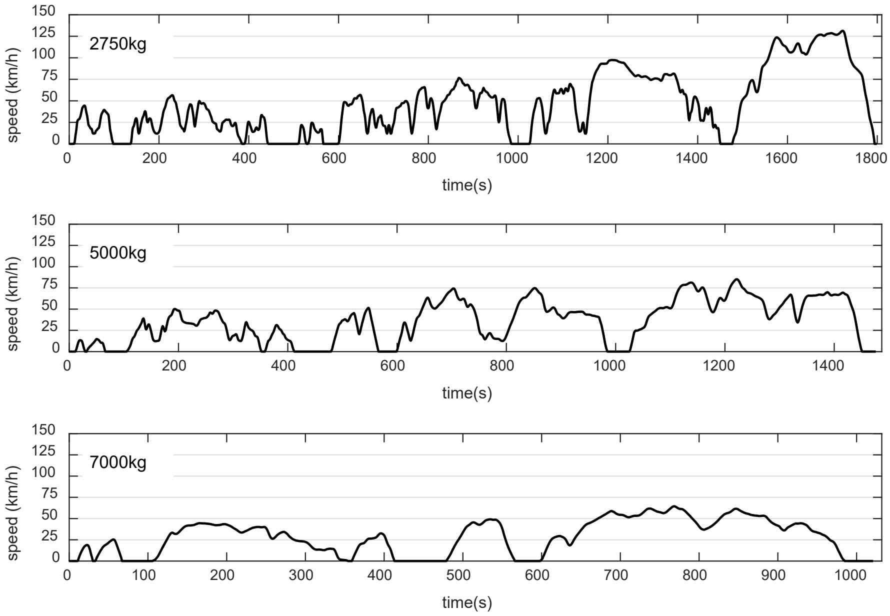

Figure 41: WLTP driving cycles for the different weight vehicles used in this report.

It must be noted that it is only optimised which gear is used and not the gear ratio. When the gear ratio is adapted to better match the particular drive train that is used, further improvements may be achieved.

The weight is a critical parameter for light commercial vehicles as it limits the possible payload. A hybrid system inevitably adds some weight to the drivetrain. Whether this additional mass (ca. 60kg) is acceptable or not depends on the specific use of the vehicle. However, in order to provide an option for a mass-neutral alternative a drivetrain with a smaller (and therefore lighter) internal combustion engine is simulated as well. In addition to the 3.0 litre F1C CNG engine that was used for all the measurements in this project, a hypothetical 2.3 litre version F1A was also used. This engine exists as a diesel engine already and it is assumed here, that it would be possible to modify that engine with little effort to operate with natural gas and that it is possible to scale the maximum torque curve with the displacement and that this does not affect the brake efficiency of the engine. Table 6 contains the masses of the components that were used for simulation.

Table 6: Masses of powertrain components used for simulation

3.0 litre F1C CNG engine	245kg
2.3 litre F1A Diesel engine (a CNG Version is assumes the same weight)	190kg
ZF 8-speed gearbox	87kg
40kW electric machine	13.33kg (specific power: 3kW/kg)
8kWh battery pack	44.44kg (specific energy: 0.18kWh/kg)

These figures show, that by reducing the engine size (-60kg) enough mass can be saved to add the hybrid system (+57.77kg). It must be noted, that we neglected the mass of the power electronics and cables etc. here, however, the weight added by those components would be rather low and is hard to quantify while at the same time the battery size is rather large for a hybrid electric vehicle (HEV).

There are HEVs on the market that have a 30kW electric machine and still only a 1.5kWh battery. The reason this is possible is the rather low power density of internal combustion engines that are used in commercial applications. The reason to choose a 40kW electric machine is that it is offered by ZF, who is also the gearbox supplier already, and that optimal fuel savings can be achieved when the power of the electric machine is approximately a quarter to a third of the engine power, which is the case here.

It is well known that there is an optimal hybridization ratio [22][23]. A too small electric machine does not provide the full benefits, whereas a too large electric machine adds unnecessary mass.

In total 6 six different drivetrains are be compared in the report:

1. Baseline 3.0 litre F1C CNG engine 100kW/350Nm (±0kg)
2. Improved 3.0 litre F1C CNG engine (Turbo + conv. camshaft) 123kW/425Nm (±0kg)
3. Improved 3.0 litre F1C CNG engine (Comprex + Miller camshaft) 123kW/425Nm (±0kg)
4. HEV: Improved 3.0 F1C CNG engine (Turbo + conv. camshaft) 123kW/425Nm, 40kW/230Nm electric machine (+60kg)
5. HEV: 2.3 F1A CNG engine, 94kW/325Nm, 40kW/230Nm electric machine (±0kg)
6. HEV: 2.3 F1A CNG engine, 94kW/325Nm,
   no Gearbox but a larger electric machine/battery 70kW/900Nm electric machine (±0kg)

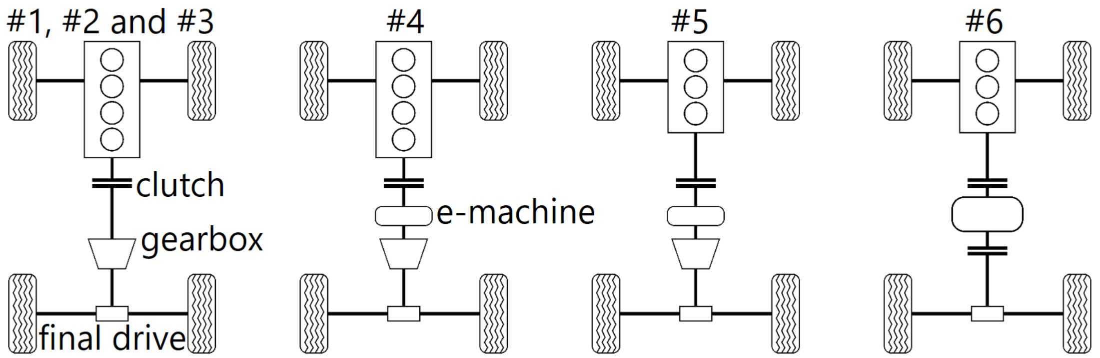

Figure 42: drive train configurations

Figure 42 gives an overview of the drivetrains of the six configurations. Drivetrains 1-3 are just the conventional drivetrain, drivetrains 4 and 5 are hybrid electric vehicles with different size internal combustion engines. Drivetrain 6 details the drivetrain with the larger electric machine that has no gearbox.

The drivetrain without a gearbox is somewhat unintuitive and therefore some more details are provided here. The idea of such a vehicle is, that the low speeds are always driven purely electric and the one gear provides sufficient potential to allow a charge sustaining operation of the vehicle if desired. In this case, the 6th gear has a gear ratio of 1 which means that the engine is operates as if it were always in 6th gear if the engine is used. This leads to a vehicle speed of 38km/h at an engine speed of 1000min^{-1}, 100km/h are driven with 2650 min^{-1} and the maximum speed at 3500 min^{-1} is 132km/h, which is acceptable for this class of vehicle. The weight (and cost) that can be saved by not using a gearbox allows for a larger electric machine and a larger battery. For this configuration, a 70kW electric machine and a 19.6 kWh battery are used and this vehicle could be used as a plugin hybrid electric vehicle (PHEV). However, the power of the electric machine is not large enough to launch the 7000kg vehicle uphill and therefore this drivetrain is only analysed for the light vehicle class.

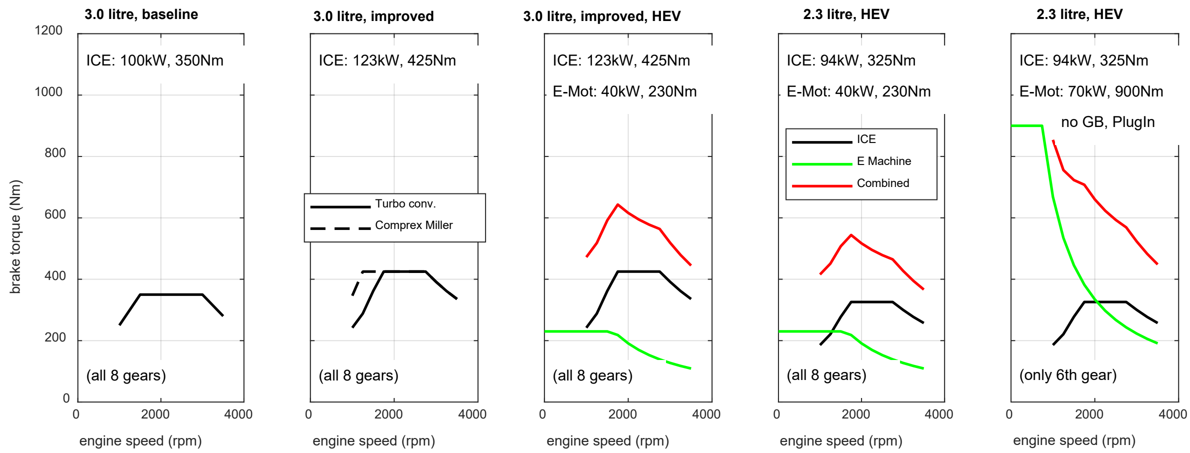

Figure 43: torque and power characteristics of the drivetrains

Figure 43 summarizes the torque and power characteristics of the drivetrains. Since one goal of the project was to improve the drivability of the vehicles, simulations are carried out to determine the acceleration of a vehicle with a weight of 2750kg. It is assumed, that the gearshifts are infinitely fast and the maximum torque of the engine is available instantly (which is more realistic if a Comprex is used instead of a turbocharger).

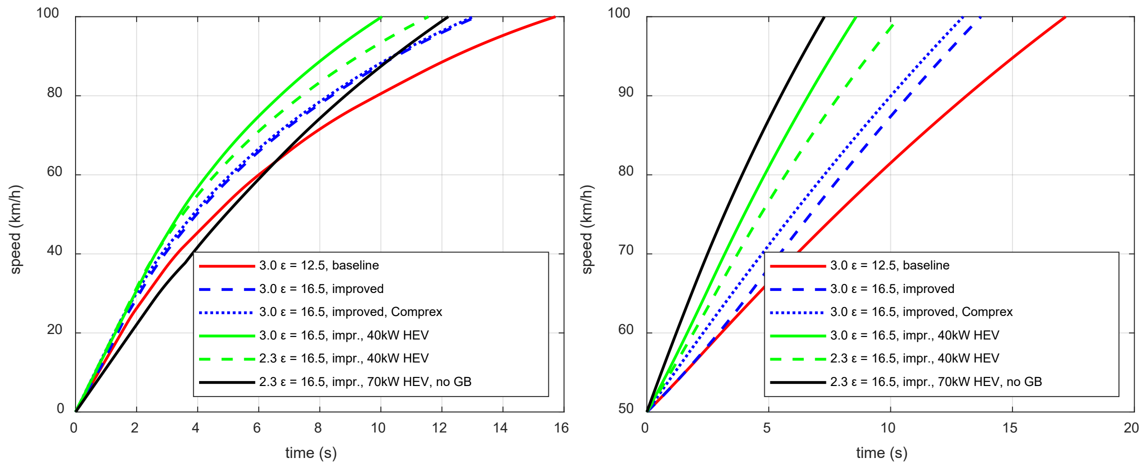

Figure 44: acceleration from 0-100km/h (left) and from 50-100km/h in 6th gear (right)

The resulting times are summarized in the table below

Drivetrain	0-100 km/h best gear	50-100km/h best gear	50-100km/h 6th gear
3.0 litre baseline	15.7s	11.1s	17.2s
3.0 litre improved	13.1s	9.2s	13.7s
3.0 litre improved, Comprex	13.0s	9.2s	13.0s
3.0 litre improved, 40kW/8kWh HEV	10.0s	6.6s	8.6s
2.3 litre 40kW/8kWh HEV	11.6s	8.0s	10.4s
2.3 litre 70kW/19.6kWh HEV, no gearbox	12.2s	7.3s	7.3s

These figures show that the acceleration from 0-100km/h is about 20% faster with the improved engine. There is almost no difference between the turbocharged engine and the Comprex supercharged engine since the low engine speeds, where the Comprex provides more torque, is only used at very low speeds and thereafter, the maximum torque curves are assumed equal. However, all hybridized vehicles are even faster than that. The HEV with the smaller combustion engine is faster than its non-hybrid counterpart with the larger engine.

The acceleration from 50km/h in 6th gear (1300rpm) represents a driving situation that often occurs in practice. Here, the vehicle without gearbox is fastest, as it has a large electric machine. Both other HEVs also benefit clearly from the additional torque provided by the electric machine and the time reduces by 50.0% and 39.5%, respectively. The improved turbocharged engine reduces the time by 20.3% and the Comprex supercharged engine due to its superior low-end torque by 24.4%.

Therefore, all drivetrains presented here provide more than 20% faster accelerations while the hybrid vehicles even provide a much higher benefit than that.

Figure 45, Figure 46 and Figure 47 show the result of the fuel consumption for the three different vehicle weights for all drivetrains. In case of the hybrid vehicles, the battery at the end of the driving cycle has the same state of charge as in the beginning (charge sustaining operation). The results are somewhat similar in that with modification of the engine alone a reduction of the fuel consumption of 7.0%, 6.8% and 7.3%, respectively, can be achieved. The engine equipped with the Comprex supercharger outperforms the turbocharged engine because of the efficiency gains due to the Miller camshaft and because a different gearshift strategy can be used due to the increased low end torque. For the hybrid electric vehicles (with gearbox) the fuel consumption benefits range from 30% up to 50% and the benefits are larger for the heavier vehicles. On one hand, the fuel savings result from the fact that the engine does not have to be operated at low loads, where the engine efficiency is lower as indicated in the plots of the engine operating points. The fuel share, that is used at these low operating points ranges from 34% to over 50%, depending on the driving cycle. On the other hand, instead of using friction brakes, the hybrid electric vehicles can charge the battery during deceleration phases.

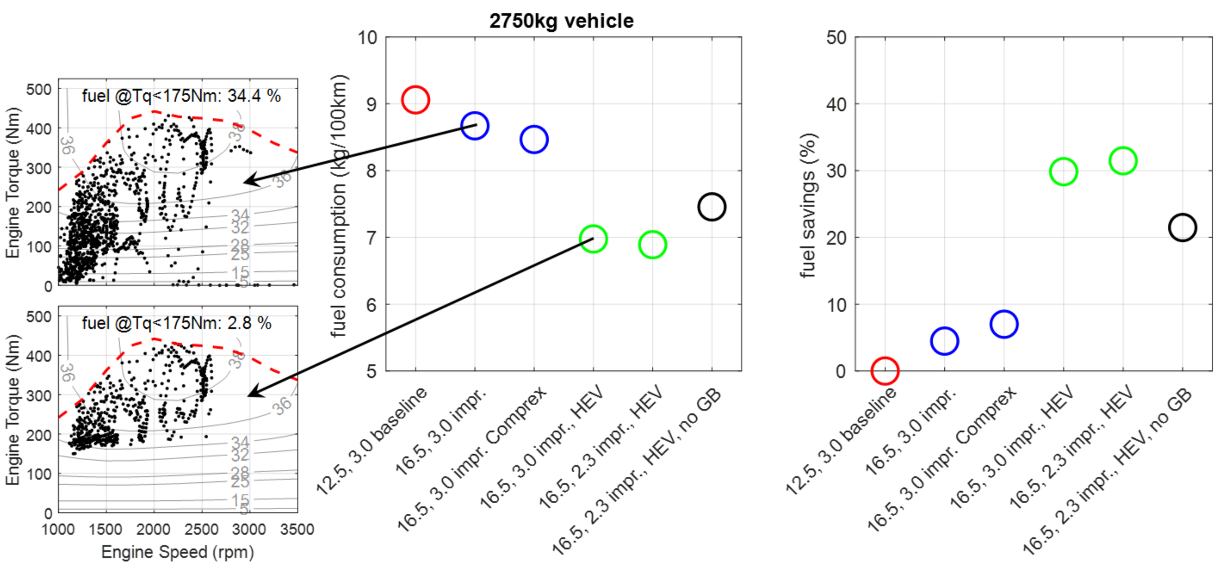

Figure 45: fuel consumption of the 2750kg vehicle for different drivetrains

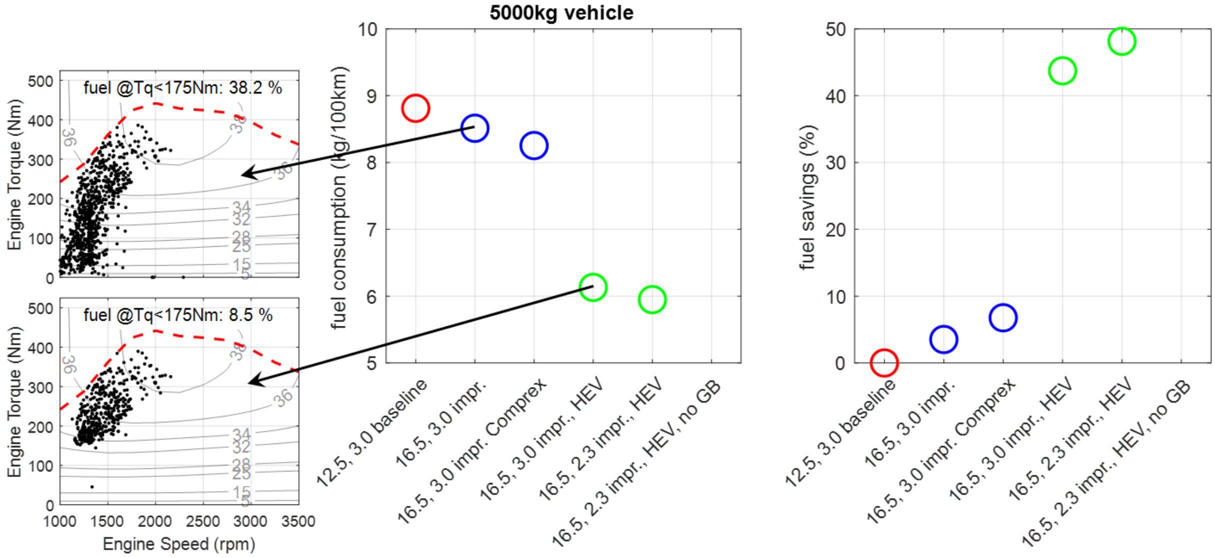

Figure 46: fuel consumption of the 5000kg vehicle for different drivetrains

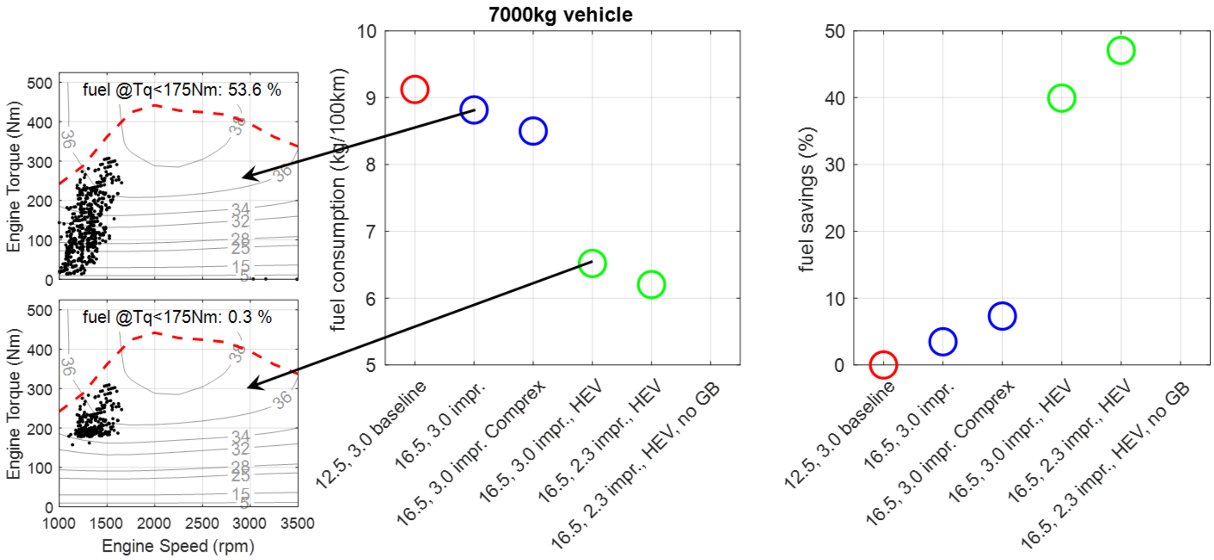

Figure 47: fuel consumption of the 7000kg vehicle for different drivetrains

The hybrid electric vehicle that has no gearbox shows lower fuel savings, because certain low speed driving situations are not possible with the engine and the times where the battery can be recharged is limited to the operation at higher vehicle speed. However, the use of the charge depleting operation, which is possible for plugin HEVs has not been taken into account here. The vehicle has an all-electric driving range of 30km in low and medium speed parts, i.e. in the first 1000s of the WLTC, shown in

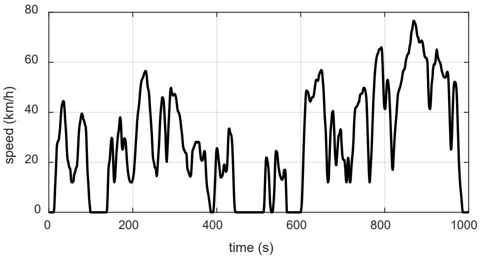

Figure 48. The battery state of charge in that case reduces from 100% to 40%. The remaining 40% are necessary, since a high electric power cannot be provided by an empty battery but a high electric power is often required for such a vehicle concept.

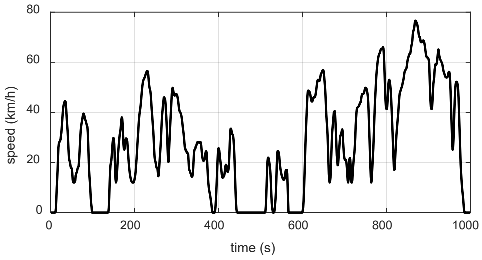

Figure 48: low/medium speed parts of the WLTC

If the battery is emptied over two WLTC cycles from 100% to 40%, the fuel consumption is 2.1kg/100km and the utility factor is 0.73. During the charge sustaining operation, the fuel consumption was 7.46kg/100km. according to the current WLTP regulations, this would lead to an overall fuel consumption of

$$C = (1-0.73) \cdot 7.46 \text{ kg/100km} + 0.73 \cdot 2.10 \text{ kg/100km} = 3.54 \text{ kg/100km}$$

The use cases, where this plugin HEV would make a significant improvement are of course limited to applications where the daily driven distance (the distance between recharges to be precise) is rather low. However, vehicles for parcel delivery often do not drive more than 200km per day. If such a vehicle can be recharged over a lunch break, the all-electric part can increase up to 60km, which is 30%. Other than a purely electric commercial vehicle, this vehicle does not have a lower payload and still has the possibility of driving large distances on the highway, which is hardly possible with purely electric light commercial vehicles.

5 Conclusions

The main project goals were to demonstrate technologies to increase the efficiency of the F1C engine for light commercial vehicles by 20% and simultaneously increase the engine's power by 20%.

These goals could be achieved. The engine's output (power and torque) could be increased 20% by the design of a new cylinder head cooling architecture (split core) and by adaptation of the turbocharger control. This is a measure which can be transferred to production in the short term. When additional technologies area applied, such as pressure-wave-supercharging and water injection, the output can even be increased further. Higher engine power and torque translate to better driveability and the possibility to change the gear ratios (i.e. running the engine at lower speed / higher load), which reduces fuel consumption.

The fuel savings/efficiency increases of engine-measured alone were identified as follows:

- In turbocharged configuration: 4.5%, 3.5%, 3.5% (in the respective driving cycles/vehicle masses), savings due to higher operating points, higher compression ratio, other gearshift strategy.
- In Comprex configuration: 7.0%, 6.8%, 7.3% (in the respective driving cycles/vehicle masses), savings due to high compression ratio, Miller camshaft and high low end torque.

20% faster acceleration (compared with today's powertrain) with engine measures alone are possible, which would help for the acceptance CNG engines.

Additional fuel savings can be realized by changing the powertrain from a pure internal combustion engine structure to a hybrid-electric structures. Detailed simulations revealed the following fuel savings/efficiency increases potentials:

- In non-plugin configuration 30…48% (higher saving for the heavier versions of the vehicle). The savings are possible to be realized weight neutral for the vehicles if a smaller ICE is used, which also results in no downside through reduction of the vehicle's payload.
- In plugin configuration 20% for vehicles up to 3500kg total weight. Also weight neutral configurations are possible with a simplified hybrid architecture without a gearbox. 30km purely electric range, may lead up to 30% electric driving for parcel delivery vehicles with low daily range of 200km (WLTC certified fuel consumption 3.54kg/100km).

Up to 40% faster acceleration for the hybrid configurations are possible, despite using a smaller combustion engine

Key takeaway messages from this project:

- CNG engines for light commercial vehicles have the potential for a similar output as modern diesel engines, key is a good cooling concept for the cylinder head.
- Enhanced boosting concepts, such a pressure-wave-supercharging, have the potential to enable excellent efficiencies (i.e. through Miller valve timing) and simultaneously increase the engine torque level as well as the dynamic response.
- Additional measures such as water injection, advanced ignition concepts and exhaust gas recirculation have the potential to increase the engine's efficiency, each measure typically increased efficiency by around 1%.
- Downsizing and hybridizing light commercial vehicles is possible, the resulting vehicle can be done mass neutral, can save more than 30% fuel and even accelerates quicker.

6 Outlook and next steps

Since the engine manufacturer FPT (FPT Motorenfoschung AG Arbon as well as FPT Torino) was involved in the project, they directly heard about all project results. FPT can use the results to further develop the engine. Which technological blocks will be used is a strategic decision of FPT which they do not communicate freely. However, each technological block needs development steps for serial production, a task which is usually done within the company.

However, the main project results were published in an open access journal [18] and are therefore available for the research- as well as for the industrial community.

An important further step for renewable fuels would be to make engines easy to adapt to different fuels. To do so, the engine has to be as flexible as possible. Within this project, we could demonstrate a very flexible alternative boosting concept – the Comprex pressure wave supercharger.

Another flexibility, which could bring large benefits, would be freely adjustable valve timing (in this project, we had to use different camshafts to perform different concepts). We are therefore planning to start a project which brings fully variable valve timing to heavy duty engines in order to gain efficiency and make them adaptable to different fuels and new combustion concepts.

7 National and international cooperation

National:

- Cooperation with FPT Motorenforschung AG, Arbon, in the field of adapted engines and engine components
- Cooperation with Antrova AG (Stein am Rhein) in the field of alternative boosting solutions.
- Cooperation with FHNW (Prof. Dr. Kai Herrmann), project work/theses for students in the framework of this project
- Cooperation with PSI / EPFL in the field of exhaust gas aftertreatment (common PhD student Moyu Wang, her experimental engine date is acquired on the F1C engine of this project).

International:

- Cooperation with FPT (Torino, Italy) in the field of series production engine components.
- Cooperation with Nostrum Energy (Ann Arbor, Michigan, USA) design of port water injection system.
- Cooperation with Politecnico di Milano with a common PoliMi-Empa PhD student (Giovanni Gianetti) in the field of CFD modeling.

8 Publications

- Rojewski J, Soltic P, Manca Di Vilhermosa G, Klein D, Gianetti G, Lucchini T, CAE Approach for Optimized EGR System in CNG Powered Engine, SCCER Mobility Annual Conference 2018, Zürich
- Rojewski J, Soltic P, Klein D, Hardy G, Skopil M, Widenhorn M, New Boostig Concept for a Methane-Powered engine, SCCER Mobility Annual Conference 2019, Zürich
- [7] Gianetti G, Sforza L, Lucchini T, Errico GD, Soltic P, Rojewski J, et al. CFD modeling of combustion of a natural gas Light-Duty Engine. Energy Procedia 2018;00:12–4.
- [24] Gianetti G, Sforza L, Lucchini T, D'Errico G, Soltic P, Rojewski J, et al. CFD modeling of natural gas engine combustion with a flame area evolution model. 74th ATI Natl Congr Energy Convers Res Innov Dev Ind Territ 2019;2191:020087 (11 pp.). https://doi.org/10.1063/1.5138820.
- [25] Sforza L, Lucchini T, Gianetti G, D'Errico G. Development and Validation of SI Combustion Models for Natural-Gas Heavy-Duty Engines. SAE Tech Pap 2019-24-0096 2019.

- [18] Zsiga N, Skopil MA, Wang M, Klein D. Comparison of Turbocharging and Pressure Wave Supercharging of a Natural Gas Engine for Light Commercial Trucks and Vans. Energies 2021;14:1–24. https://doi.org/https://doi.org/10.3390/en14175306.
- [20] Wang M, Dimopoulos Eggenschwiler P, Franken T, Ferri D, Kröcher O. Reaction pathways of methane abatement in Pd-Rh three-way catalyst in heavy duty applications: A combined approach based on exhaust analysis, model gas reactor and DRIFTS measurements. Chem Eng J 2021;422. https://doi.org/10.1016/j.cej.2021.129932.
- [26] Wang M, Dimopoulos Eggenschwiler P. Modeling of three way catalyst behavior under steady and transient operations in a stoichiometric natural gas fueled engine. SAE Tech Pap 2021-24-0074 2021.
- Norbert Zsiga et al.: Hybridization of light commercial vehicles – currently being written
- Giovanni Gaetano Gianetti, 3D CFD Modeling of Premixed Combustion in Natural Gas engines, Doctoral Dissertation, Politecnico di Milano, defense 07.09.2021

9 References

[1] Natural Gas Vehicles in Europe. CNG Eur n.d. http://cngeurope.com/natural-gas-vehicles/.

[2] 2020 Gas Vehicles Statistics. Https://WwwNgvaEu/Wp-Content/Uploads/2021/04/NGVA-Europe_PRESS-RELEASE_2020-Gas-Vehicle-StatisticsPdf 2021.

[3] CNG Tankstellen in der Schweiz. Https://WwwCng-MobilityCh/Finden-Sie-Cng-Tankstellen-in-Ihrer-Naehe/ n.d.

[4] Bach C, Bütler T, Soltic P. Erdgas/Biogasfahrzeuge im Kontext der Energiestrategie 2050 und der CO2-Gesetzgebung. 2014.

[5] European Parliament And The Council Of The European Union. Regulation (EC) No 595/2009 on type-approval of motor vehicles and engines with respect to emissions from heavy duty vehicles (Euro VI) and on access to vehicle repair and maintenance information and amending Regulation (EC) No 715/2007 and Directive 2007. Off J Eur Union 2009;L 188:1–13.

[6] FPT Industrial F1A and F1C Engines for the New IVECO Daily “Bluepower” n.d. https://media.cnhindustrial.com/EUROPE/FPT-INDUSTRIAL/fpt-industrial-f1a-and-f1c-engines-for-the-new-iveco-daily--bluepower-/s/ff84bc56-fd41-452d-b4a5-2d5216ff3af3.

[7] Gianetti G, Sforza L, Lucchini T, Errico GD, Soltic P, Rojewski J, et al. CFD modeling of combustion of a natural gas Light-Duty Engine. Energy Procedia 2018;00:12–4.

[8] Gianetti G, Sforza L, Lucchini T, D’Errico G, Soltic P, Rojewski J, et al. CFD modeling of natural gas engine combustion with a flame area evolution model. AIP Conf. Proc., vol. 2191, 2019. https://doi.org/10.1063/1.5138820.

[9] GT-POWER Engine Simulation Software n.d. https://www.gtisoft.com/gt-suite-applications/propulsion-systems/gt-power-engine-simulation-software/.

[10] Toulson E, Schock HJ, Attard WP. A Review of Pre-Chamber Initiated Jet Ignition Combustion Systems. SAE Tech Pap Ser 2010;1. https://doi.org/10.4271/2010-01-2263.

[11] Bolla M, Shapiro E, Kotzagianni M, Kyrtatos P, Tiney N, Boulouchos K. Numerical study of fuel and turbulence distributions in an automotive-sized scavenged pre-chamber. Combust Engines 2019;176:61–7. https://doi.org/10.19206/CE-2019-108.

[12] Soltic P, Hilfiker T, Hänggi S. Efficient light-duty engine using turbulent jet ignition of lean methane mixtures. Int J Engine Res 2019. https://doi.org/10.1177/1468087419889833.

[13] Multitorch GmbH Industrial Spark Plugs n.d. https://www.multitorch.de/.

[14] Akbari P, Nalim R, Mueller N. A review of wave rotor technology and its applications. J Eng Gas Turbines Power 2006;128:717–35. https://doi.org/10.1115/1.2204628.

[15] Hauri S. Der bessere Turbolader kehrt zurück. NZZ 2021.

[16] Comprex(TM) Druckwellenlader n.d. https://www.antrova.com/comprex-tm-druckwellenlader.

[17] Skopil MA. Hydrogen Engines and the New Comprex^{TM} Pressure Wave Supercharger Concept. 42nd Int Vienna Mot Symp 2021.

[18] Zsiga N, Skopil MA, Wang M, Klein D. Comparison of Turbocharging and Pressure Wave Supercharging of a Natural Gas Engine for Light Commercial Trucks and Vans. Energies 2021;14:1–24. https://doi.org/https://doi.org/10.3390/en14175306.

[19] Skopil MA. Hydrogen engines and the new Comprex^{TM} pressure wave supercharger concept. Youtube n.d. https://youtu.be/QMNIlhXNN6g.

[20] Wang M, Dimopoulos Eggenschwiler P, Franken T, Ferri D, Kröcher O. Reaction pathways of methane abatement in Pd-Rh three-way catalyst in heavy duty applications: A combined approach based on exhaust analysis, model gas reactor and DRIFTS measurements. Chem Eng J 2021;422. https://doi.org/10.1016/j.cej.2021.129932.

[21] Hutter R, De Libero L, Elbert P, Onder CH. Catalytic methane oxidation in the exhaust gas aftertreatment of a lean-burn natural gas engine. Chem Eng J 2018;349:156–67. https://doi.org/10.1016/j.cej.2018.05.054.

[22] Sundström O, Guzzella L, Soltic P. Torque-assist hybrid electric powertrain sizing: From optimal control towards a sizing law. IEEE Trans Control Syst Technol 2010;18:837–49. https://doi.org/10.1109/TCST.2009.2030173.

[23] Sundström O, Guzzella L, Soltic P. Optimal hybridization in two parallel hybrid electric vehicles using dynamic programming. IFAC Proc. Vol., vol. 17, 2008. https://doi.org/10.3182/20080706-5-KR-1001.2452.

[24] Gianetti G, Sforza L, Lucchini T, D'Errico G, Soltic P, Rojewski J, et al. CFD modeling of natural gas engine combustion with a flame area evolution model. 74th ATI Natl Congr Energy Convers Res Innov Dev Ind Territ 2019;2191:020087 (11 pp.). https://doi.org/10.1063/1.5138820.

[25] Sforza L, Lucchini T, Gianetti G, D'Errico G. Development and Validation of SI Combustion Models for Natural-Gas Heavy-Duty Engines. SAE Tech Pap 2019-24-0096 2019.

[26] Wang M, Dimopoulos Eggenschwiler P. Modeling of three way catalyst behavior under steady and transient operations in a stoichiometric natural gas fueled engine. SAE Tech Pap 2021-24-0074 2021.